AN EXPERIMENTAL STUDY OF

BLADE TIP VORTICES

By: Raymond Piziali & Andrew Trenka

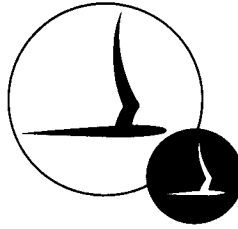# CAL No. AC-2647-S-1

Prepared For:

National Aeronautics and Space Administration
Langley Research Center
Langley Station
Hampton, Virginia   23365

FINAL REPORT

NASA Contract NAS1-8117

January 1970

AN EXPERIMENTAL STUDY OF BLADE TIP VORTICES

By Raymond Piziali and Andrew Trenka

CAL Report No. AC-2647-S-1

CONTENTS

LIST OF FIGURES

v

SUMMARY

An initial experimental investigation was conducted to determine the influence of tip shape on the tip vortex formation and the aerodynamic performance of lifting surfaces representative of typical helicopter rotor blades. The objective was to assess the potential for beneficially altering the generation of the tip trailing vorticity by proper design of the tip. Flow visualizations and force measurements were made in a wind tunnel on a semi-span model wing at free-stream velocities of nominally 100 fps. Six different tip configurations were investigated at free stream velocities of nominally 100 fps. The wing had a NACA 0012 airfoil, a 13 3/4 inch semi-span, and a constant 3 1/2 inch chord except at the tip. The test Reynolds number was nominally 190,000.

The external flow about the tip was visualized with an oil smoke and the surface flow with a pigmented oil. Some of the results of both visualization techniques are presented and discussed for each tip configuration. An additional sequence of smoke flow photographs which clearly show the details of the tip vortex formation on a square tip is also presented. As judged from the flow visulaizations, the tip vortex apparently becomes more concentrated and forms farther outboard in the wake as the lateral edge of the tip is more closely aligned with the free stream direction.

The force results are presented and discussed, however, their value has been discounted because of their sensitivity to small changes in the pressure distribution arising from unpredictable changes in the wing boundary layer flow. This problem was anticipated and it was thought that it could be substantially alleviated by the use of a boundary layer trip. However, for this airfoil and the attainable Reynolds number range, attempts to do so were not successful.

The qualitative character of the local flow in the vicinity of the tips and tip vortices was not observed to be sensitive to the relatively small changes in the overall wing pressure distribution which have invalidated the force data. Thus, the flow visualizations are believed to provide a valid characterization of the tip flow field and a useful insight into the nature of the three-dimensional tip flow field.

It has been concluded that, by proper design of the wing tip, it should be possible to beneficially alter the generation of the tip trailing vorticity. The benefit realized from this alteration would be in the form of reduced induced velocities in the wake and/or reduced induced drag of the lifting surface. However, no data were obtained which allowed any definitive statements relative to the magnitude of the benefits nor whether they can be achieved simultaneously. It is, therefore, recommended that more quantitative investigations be made. These investigations should include the measurement of wing forces and moments and the induced velocities in the wake.

INTRODUCTION

Helicopters have always been characterized by the vibration and noise generated by their rotor systems. The vibration environment greatly increases maintenance costs and the rotor noise is not only objectional to the personnel involved in a flight but can be extremely detrimental in attack missions by supplying the enemy with an early warning of the impending attack.

Another characteristic of helicopters is the small payload-to-gross weight ratio. As a result of this ratio, small reductions in the power required will yield relatively large increases in the payload. This problem is even more critical in the V/STOL vehicles with highly loaded lifting propellers.

It is generally accepted that the operating characteristics of rotating-wing devices such as helicopter rotors, aircraft propellers, and V/STOL propeller rotors are strongly influenced by their vortex wakes. The aerodynamic loads experienced by the individual blades of these devices, and thus their operating performance, vibration, and noise characteristics, are dependent upon the complex vortex wake through the angle-of-attack distribution as influenced by the wake-induced velocities. This wake, which is shed by the individual blades, is generated as a helical sheet of shed and trailing type vorticity. However, the trailing vorticity is much stronger than the shed vorticity and it very quickly becomes concentrated or rolled up in the region behind the tips into what is commonly referred to as trailing tip vortices. It is these trailing tip vortices which make up the significant part of the rotating wing wake.

The distribution of the trailing vorticity immediately behind a blade not only depends upon the spanwise loading distribution but at the same time determines it. Thus, the induced drag is strongly dependent upon the distribution of trailing vorticity near the blade.

With respect to the rotor noise problem, it has been conjectured that blade "slapping" or "banging" is the result of very rapid time rates of change in the local blade pressure distribution due to the angle-of-attack change which occurs when a blade passes through or very close to a trailing tip vortex from a preceding blade. Such an incident, under the proper operating conditions, could also cause the formation of a local normal shock wave on the outer portion of the blade. This might also be a source of blade slap noise. Thus, blade slap would be dependent upon the maximum induced velocities encountered by the blades. The maximum induced velocity encountered by the blades would depend upon the proximity of the blades to the concentrated trailing vortex elements deposited in the wake by preceding blades and the relative concentration (core size) of these vortices. The

2

relative concentration and location of this trailing vorticity in the wake are influenced by the manner in which the vorticity is generated and rolls up.

The wake vorticity of a blade (a rotating wing) is generated in the boundary layer by the viscous action of the air. The "trailing" components of the wake vorticity are the result of the spanwise pressure gradients and these are greatest in the region of tips. Thus, if by proper design of the blade tips this tip flow could be controlled, it might be possible to exercise some control over the distribution of the trailing vorticity and its influence on the performance, vibration, and noise of rotor systems.

Because the flow in the region of the tips is relatively independent of the flow over the remainder of a wing, it can be argued that, for the same tip design, the flow about wing tips is virtually the same as that about the tips of rotor blades in the hovering and low advance ratio operating condition. Therefore, the much simpler investigation of the flow about the tips of a wing will yield results which are representative of that about rotor blade tips.

Thus, an experimental investigation was undertaken with the objectives of 1) determining the influence of wing tip geometry on the distribution of trailing vorticity shed from the tips and on the wing drag (profile plus induced), 2) improving the physical understanding of the tip flow (i. e. , generation of the tip vortex), and 3) indicating the potential benefits of altering the generation of the tip trailing vorticity.

To accomplish these objectives, wind tunnel tests were conducted in which smoke flow and surface oil flow studies were made on a model wing. Force measurements were also made. The primary parameter which was varied was the shape of the wing tip.

In addition to the experimental effort, a brief literature search was made during this investigation relative to the subject of wing tips and tip vorticity. The results of this search are presented in the Bibliography. Two of these reports are of particular interest. One is "Flow Separation in Three Dimensions" by Maskell (Reference 1) which presents a very enlightening discussion of the generalized concept of flow separation. The other is "Axial Flow in Trailing Line Vortices" by Batchelor (Reference 2) in which the idea of the rolling up of the trailing vorticity is related to radial inflow, axial acceleration in the core, and the rate of change of the circulation about the vortex.

DESCRIPTION OF EXPERIMENTAL APPARATUS

Test Facility

The tests were conducted in the subsonic leg of the CAL/Air Force High-Speed Wind Tunnel. Figure 1 is a planview of this facility. The subsonic leg forms a low turbulence, non-return tunnel with a 17" x 24" test section. The tunnel is capable of testing at speeds up to about 125 feet per second. The low turbulence level is obtained by use of a high contraction ratio entrance bell preceded by a series of three fine-mesh turbulence screens. Additional smoothing of the entrance flow is provided by cheese cloth stretched over a 6' x 8' x 5' frame in front of the bell and screens; the cheese cloth also acts as a large area filter which substantially reduces the cleaning requirements of the turbulence screens.

The 17" x 24" test section is approximately 32 inches in length and each of its sides is a removable plexiglass **window**. On top, the test section width is spanned by a smaller (10" x 17") plexiglass window. The top and bottom of the test section are made slightly divergent (approximately 0.5 degrees each) to compensate for the growth of the boundary layer on the test section walls.

Models

The model tested was a constant chord, untwisted, semi-span wing with six interchangeable tip sections. It was mounted vertically so that the test section floor served as the reflection plane. Several photographs of the wing and installation are presented in Figure 2.

The wing has a NACA 0012 airfoil section, a 3 1/2-inch chord, and a 13 3/4-inch span (except for one model of the blunt square configuration which had a 14-inch span).

The wing was fitted, via an adapter, to an available six-component, strain-gauge sting balance and the combination was cantilevered from a pair of bearings below the test section floor. The balance was oriented with respect to the wing so that it measured the wing normal force, chord force, etc. A coordinate transformation was required to obtain the lift, drag, etc. in the wing-axis system. An arm was clamped to the sting to enable changing the angle of attack by rotating the wing-balance combination in the bearings. The angle of attack was set by inserting an alignment pin through a hole in the arm into one of a sequence of accurately located holes in an adjacent plate.

To enable the use of suction for controlling the test section wall boundary layer in the region of the wing root, an area (approximately 3" x 5") of the floor about the wing root was perforated with 1/8-inch holes and a plenum was installed below the floor to enclose this area. The gap between the wing and wall was set to about 0.005 inches at the leading edge; it was somewhat more at the trailing edge due to the slight divergence of the top and bottom of the test section.

The outer 3 1/2-inches of each wing configuration was a replaceable tip section. These tip sections were carved from balsa wood bonded to an aluminum chord plate with a projecting tongue which fit into the outer end of the wing. The tips were constructed so that there was no spanwise variation of the profile thickness ratio. Photographs of the six tips are presented in Figure 3. The rounded square tip configuration wing is a rectangular planform with a tip cap formed by rotating the airfoil section about its chord line; the 13 3/4-inch span of the wing is measured to the outer edge of the tip cap. The blunt square tip configuration wing is a rectangular planform with the tip cut off normal to the chord plane. The 45-degree swept forward tip configuration wing has a straight leading edge with the trailing edge swept forward at 45 degrees to a pointed tip; the 60-degree swept forward tip is similar except the trailing edge sweep is 60 degrees. The 45-degree swept aft tip configuration wing has a straight trailing edge and the leading edge is swept aft at 45 degrees to a pointed tip. The cusp tip configuration wing has a straight leading edge and the trailing edge for the outer 3 1/2-inches of span is contoured to form a cusp at the tip. The area of each wing configuration is given in Table I.

TABLE I

Tip	Area(inches^2)
Rounded square	47.9
Blunt square	48.1
45-degree swept forward	42.0
45-degree swept aft	42.0
60-degree swept forward	45.1
Cusp	41.2

The wing and all the tips were given a smooth high gloss black finish and, for increased visibility, a thin white line was applied around the entire outline of the model. For all, except some of the initial preliminary runs, the wing and tips had a boundary layer trip on both surfaces. This trip consisted of a distribution of #80 carborundum grit bonded to the forward surface of the wing along a spanwise band about 0.4 inches wide.

Smoke Generator and Probes

The smoke generating system, used in this program, is basically a commercial smoke producer connected to the smoke probe via flexible plastic tubing, oil traps, and an overflow. Photographs of this system are presented in Figure 4. The smoke is in reality an oil fog, that is, a suspension of liquid oil droplets in a mixture of air and oil vapor. It is generated by the mixing of a supersaturated oil vapor with air. The physical processes involved in generating this smoke are discussed in Appendix A.

The commercial smoke producer itself is small, compact, reliable, and simple to operate. It contains a small tank (2-1/2-lb. size) of compressed CO_2 gas with pressure regulator and gauges. The CO_2 provides the vehicle and pressure to carry the oil from the internal 200 cc. reservoir through a fixed metering assembly to an internal electrically heated vaporizer and out the discharge nozzle. The pressure regulator setting on the CO_2 tank controls the quantity (rate) of smoke produced. The flow of the CO_2 and thus smoke production are turned on and off by a toggle operated valve. The vaporizer heat is turned on and off by a toggle switch and is regulated by a thermostat to maintain a temperature of 650 degrees Fahrenheit. The unit requires an initial 20 minute warm-up period; thereafter the smoke production is turned on and off at will via the toggle valve.

The saturated oil vapor jet issuing from the discharge nozzle condenses and produces large amounts of very dense white smoke upon entraining and mixing with the external body of air. However, connecting the smoke producer directly to the remainder of the system via a tubing adapter (a short piece of 1/4-inch in diameter steel pipe attached to the discharge nozzle) eliminated the external air and thus virtually eliminated the smoke production. This was remedied by injecting air into the vapor jet close to the discharge nozzle. While this produced an acceptable quantity of smoke for these experiments, it was considerably less than that produced by the unit operating into the open atmosphere. A larger and more efficient air-vapor mixing chamber at the discharge nozzle would be desirable.

The 2-1/2-lb. tank of compressed CO_2 was replaced with a much larger tank of nitrogen to obviate repeated replacement due to the large amount of use anticipated. Nitrogen was chosen because it was readily available in the large tank size required. Its density is also closer to that of air than that of CO_2. There was no observable difference in the smoke produced using nitrogen from that produced with CO_2. The only apparent requirement on the gas in this unit is that it not react with the hot oil vapor.

The remainder of smoke generating system consists of two glass jar oil traps, an overflow line, and the interconnecting 3/8-inch Tygon tubing. The first trap was located about 6 inches from the vapor discharge nozzle and the second trap about 18 inches beyond the first. There are two outlets from the second trap, one for the tubing to the probe and the other for the overflow line; both were fitted with adjustable tubing clamps to control the flow of

6

smoke. The two relatively large traps close to the smoke producer served not only to trap the oil collecting in the tubing adapter and lines close to the nozzle but more importantly to cool the smoke by radiating heat. This cooling process results in the condensation and collection of a relatively large amount of oil on the glass walls of the traps, thereby significantly reducing the problem of oil collecting in the 10-foot length of tubing to the probe.

The oil used is the light weight grade of mineral oil (liquid petrolatum) with a specific gravity range 0.83 - 0.86. The smoke probe shown in Figure 5 consisted of a 3/8-inch diameter glass nozzle about 4 inches long which was mounted at the end of a long, thin piece of wood. The 3/8-inch plastic tubing from the second oil trap is connected directly to this nozzle and it is taped along the upstream edge of the probe. This probe assembly was mounted on a fixture which held the probe directly in front of the turbulence screens so that the nozzle was less than one inch from the front screen and its position could readily be adjusted.

The location of the smoke probe ahead of the screens was selected after trying to insert the smoke into the airstream at three other locations; namely,

1. the test section,

2. mid-way downstream in the entrance bell, and

3. at the entrance to the bell but downstream of the screens.

The resulting smoke stream was progressively improved as the location was moved upstream; the smoke stream became significantly smaller, less diffuse and more laminar. This improvement apparently results from the action of the favorable pressure gradient (in the entrance bell) in damping the turbulent mixing of the internal("pipe") probe flow with the main stream. Moving the probe from the downstream to the upstream side of the screens produced further improvement as the screens reduced the scale of this initial mixing turbulence. The resulting smoke stream generally had a striated laminar appearance which greatly enhanced the visualization.

A brief effort was made to develop a hand-held smoke probe, or wand, which could be used to investigate the flow locally in more detail. The wand consisted of a straight length of 1/4-inch diameter stainless steel tubing terminating with a length (about 4 inches) of smaller diameter tubing bent at the end to form the nozzle; several sizes (from 1/8-inch down to 1/32-inch) of tubing for the nozzle piece were tried. The wand entered the test section from above through a hole with a flexible seal. The resulting smoke stream was diffuse and less dense than desired but certainly useable. The real problem experienced with the wand was the profuse amount of oil dripping from the nozzle. A brief attempt to reduce the amount of oil condensing in the probe by electrical heating of the probe was not successful.

EXPERIMENTAL TECHNIQUES

Calibration

Force balance. - The six-component balance was calibrated by the CAL Transonic Wind Tunnel Department using techniques developed by them for general application to the wide variety of balances which they encounter. The technique is described briefly below.

The balance was mounted on a specially constructed rig which allowed the application of known, calibrated loads (and moments) at known positions and in known directions. A loading fixture was constructed and mounted on the balance which allowed the application of the calibration loads in approximately the same relative location as the resultant airloads. The calibration loads were applied and the output from the balance recorded digitally. This procedure was repeated several times. The results were analysed using a least-square-fit technique to obtain a loading matrix. The elements in the matrix relate the applied loads to the balance output in arbitrary meter units. The scale of the meter units is fixed by applying a prespecified unbalance to each bridge circuit of the balance.

Repeated calibrations were performed with the wing mounted on the balance and installed in the test section. These were performed to check that the balance installation, wing mounting, and electrical hook up were correct. They also provided a measure of the balance repeatability and reliability.

The error associated with the balance loads of primary interest, namely, normal force and chord force are +3% on normal force and +4% on chord force as deduced from the calibrations.

Since the balance loads are presented in coefficient form and in a wind axis frame of reference, the above noted errors cannot be directly associated with results presented. To establish the errors to be associated with the presented data, an error analysis was formulated. The analysis included the estimated errors associated with the measurement of not only the wing airloads parallel and perpendicular to the chord but also the wing area, tunnel dynamic pressure and wing angle of attack.

The use of the largest estimated error in each of the above parameters yielded an error of +5% in the lift coefficient (C_L) while the corresponding drag coefficient (C_D) estimate yielded 19%. The large estimated error in the drag coefficient is directly attributable to the component of the normal force resolved into the drag direction. When the normal force is large, its contribution to the loads in the drag direction becomes a major portion of the total force. The maximum estimated error

in C_D around $C_L = 0$ is approximately ±6%.

Wind tunnel dynamic pressure. - A thorough calibration of the wind tunnel flow was completed just prior to the entry of the tests being reported herein. A survey of the flow field in the test section was made at that time as well as the calibration of a control manometer. This manometer was located at the wind tunnel control panel. The control manometer read the wall static pressure at a point approximately 2.5 inches downstream of the beginning of the test section. The reading from the control manometer in inches of alcohol was plotted against the test section dynamic pressure measured in psi. Subsequently, the control manometer was used to nominally set the tunnel dynamic pressure.

In order to facilitate data taking and obtain a more accurate reading of the dynamic pressure, an additional manometer was installed at the test section. This manometer also read the wall static pressure in the test section and it was calibrated against a pitot-static tube mounted on the tunnel center line. The reading from this manometer was in millimeters (mm) of alcohol and was the quantity from which the tunnel dynamic pressure was determined.

The estimated error in measurement of tunnel dynamic pressure is ±1%.

Wing angle of attack. - As explained previously the wing angle of attack was set by inserting an alignment pin through a hole in the angle of attack arm into a hole in the base plate of the plenum chamber (see Figure 2). The hole pattern in the base plate was drilled to give 1-degree increments in angle of attack. The location and drilling of the pattern was done on a dividing head of a milling machine which could be located to within ±5 minutes. The wing was oriented with respect with this hole pattern by aligning the chord plane with the split in the porous plate of the tunnel floor. This split lay on the tunnel center line.

The overall accuracy of the angle-of-attack measurement is estimated to be ±0.2 degrees.

Force Measurements

For each wing tip configuration the following procedure was employed to obtain the airloads. With the angle of attack set at zero and no air blowing in the tunnel, the atmospheric temperature (T) and pressure (P) were recorded, and the balance data were taken to establish tares. The wall boundary layer suction level was always set at 50 mm of alcohol except as noted in the discussion of results. This suction level was chosen as providing the most reasonable flow in the region of the wing-wall juncture as judged

from surface flow visualizations. The tunnel dynamic pressure was then brought to the desired value (nominally 0.1 psi). The angle of attack was then indexed in 1-degree increments up to stall (approximately 13 degrees) for positive angles of attack and back to zero in 2-degree increments. The process was repeated for negative angle of attack. Balance data were recorded at each angle of attack.

The balance data were recorded digitally on the same system with which the balance was calibrated as described under the Calibration procedures. The digitally recorded signals were fed into a data reduction program which computed the airloads and also converted the airloads to coefficient form in both the balance and wind frames of reference. The program provided tabulated results as well as plots of the wing loads and moments in coefficient form versus angle of attack and conventional wing lift-drag polars.

Flow Visualizations

Surface oil flow. - The procedure for the surface flow studies began first with the setting of the wall suction level (at 50 mm of alcohol), the starting of the wind tunnel, and then bringing the test section velocity up to an "idling" speed of about 5 fps. with the test section side window off. A relatively uniform coat of the oil mixture was then applied to the model surface using a soft bristled paint brush. Immediately following the application of the oil, the window was quickly put in place as the wind tunnel flow was accelerated up to the test velocity (about 100 to 115 fps). Several photographs (overall and close-up) of the oil flow pattern were then taken using a hand-held 35 mm single lens reflex camera. The test section velocity was returned to the idling speed, the window removed, the angle of attack changed, the model surface re-coated, and the process repeated for each angle of attack. The surface flow patterns were generally photographed at the following angles of attack: 0 degrees, +1 degree, +2 degrees, +4 degrees, +6 degrees, and +10 degrees. However, direct observation of the surface flow patterns was usually made over the entire angle of attack range up to and including the positive and negative stall angles.

The oil mixture used in this investigation was white artist oil paint diluted with diesel oil. This mixture did not dry on the model even over a period of a few days. The dilution was arrived at by trial and error to obtain satisfactory flow patterns. Kerosene was tried in place of the diesel oil but it would evaporate too fast and tend to "set" the initial(starting) flow pattern. French chalk was tried in place of the oil paint but it would not flow as easily as the paint and would also tend to "set" the initial pattern as the oil evaporated. Fluorescent oil and ultra-violet light were tried and

10

provided satisfactory results. However, the pattern was relatively dim and the care required in working with the strong ultra-violet light source made this method awkward.

Smoke flow. - The smoke flow visualization studies were relatively simple to conduct, and it was possible to obtain good results up to the maximum speed capability (about 125 fps.) of the wind tunnel. The procedures followed during the smoke tests are described below.

With the desired test section velocity and wing angle of attack set, the smoke generator was turned on and the position of the smoke probe adjusted until the smoke stream was nominally in the desired location relative to the wing. Small variations in the location of the smoke stream over the model would occur due to flow variations at the probe location in front of the turbulence screens. Thus, by taking many photographs for a single probe position, many different visualizations of the same local flow were recorded.

Photographs of the smoke flow downstream of the wing as well as close-ups of the smoke flow about the wing tips were taken. Most of the smoke flow visualization photographs were taken for a relatively high wing angle of attack (arbitrarily chosen as $\alpha = \pm 10$ degrees) because the characteristics of the tip flow were more pronounced at the higher angles and yet appeared virtually the same as for the lower angles of attack.

The major difficulty encountered in the smoke flow visualizations was attributed to the condensation of oil from the smoke (an oil fog) on the turbulence screens. After a period of running, the density and location of the smoke stream would begin to fluctuate and appear to be smeared out (e.g. as observed in Figure 29 (b)).

Photography

The camera used for both the surface oil flow and smoke flow visualizations was a 35 mm single lens reflex camera. Its small size, large capacity (36 exposures), relatively great depth of field (focus), lack of parallax, fast operation, and ability to focus on objects as close as 18 inches made it ideal for this assignment. It was hand held to allow the quick flexibility of view point.

The film used had a high speed (ASA 200, allowing the use of smaller lens openings and therefore greater depth of field) and a relatively fine grain size (allowing adequate enlargement of the relatively small 35 mm image). The proper exposure was determined by a series of test exposures. The density

11

range in the negatives of the smoke flow photographs generally exceeds the capability of the print papers. Thus, for some photographs of special interest several prints were made with successively greater average density. This enabled more of the information of the photographs to be observed.

The illumination for the smoke flow photographs was through the top window of the test section and was supplied by an electronic flash unit mounted in a fixed position (Figure 6). The electronic flash provided the very short exposure time required to partially freeze the smoke pattern and a strong illumination which enabled the use of small lens openings, thereby increasing the depth of field. Because background illumination will reduce the contrast of smoke visualization, two baffles (painted flat black) were installed between the electronic flash and the window (as seen in Figure 6) to restrict the light to the plane of interest. (Collimated light would be more desirable).

The surface oil flow patterns were also illuminated through the test section top window. In this case the light was from the continuous illumination of a photo-flood also used for the direct viewing.

The visibility of the smoke was greatly increased by the following procedures. The wing and tips were painted a high gloss black, and the test section walls and floor were painted a flat black (gloss black would be better in the test section if the surface reflections can be controlled). An observation booth with a knee length black curtain all the way around was fitted to the viewing side of the test section; the viewer was thus in a dark room. This prevented light from entering the test section from the viewing side and virtually eliminated the first surface reflections from the viewing window. A box-like enclosure (painted black inside) was fitted outside of the window on the opposite side of the test section; this allowed virtually all the light passing through it to be absorbed (as looking into a dark room through an open door). Both of these windows were kept highly polished; this virtually eliminated specular reflections from their surfaces. Each of these items reduced the light reflected to the viewer from surfaces other than the smoke.

12

DISCUSSION

General

The steady motion of a solid body through a fluid establishes a pressure field and a corresponding irrotational field of disturbance velocities both of which move with the body. Due to the viscosity of the fluid and the requirement that, at the surface, no relative velocity exists between the fluid and the surface, the body is completely sheathed by a relatively thin layer of fluid. In this layer the viscous shearing forces are significant and the velocity distribution is rotational. It is within this thin layer of fluid that all the vorticity of the wake is generated. Thus, all the shed and trailing type vorticity of the wake has its origin in this boundary layer of rotational fluid.

For the wing, this layer of rotational air (vorticity) generally leaves from the upper and lower surfaces along its trailing and lateral edges as a free sheet of vorticity. The strength of this resultant sheet at each point is determined by the net change in velocity across its thickness. Along the trailing edge of the wing, the free sheet of vorticity is the combination of the upper and lower layers of rotational (boundary layer) air. In steady flow the streamwise velocity components at the edge of the boundary layer on the upper and lower surface at the trailing edge are equal (the Kutta condition). Therefore, because the net change in the streamwise velocity component across the vortex sheet is zero, the shed component of vorticity it represents is also zero. (It is noted that although the net shed vorticity component is zero, it has a distribution through the sheet from the upper and lower surface boundary layer which represents the momentum defect of the wake). However, due to the spanwise pressure gradients over the surfaces of the wing, the spanwise component of the velocity at the edge of the boundary layer on the upper and lower surfaces at the trailing edge will not be equal. The change in the spanwise velocity component across the resulting free vortex sheet at the trailing edge represents the strength of its trailing component of vorticity. Because the spanwise pressure gradients are large over the outer section of the wing, especially in the region of the wing tips, the major portion of the wing trailing vorticity is from the tips and the outer wing sections. These spanwise pressure gradients and the flow adjust so as to allow the positive pressures of the lower surface and the negative pressures of the upper surface to equalize at the lateral edges of the wing as well as at the trailing edge.

The sheet of vorticity (boundary layer air) streaming from the wing very quickly becomes concentrated into a streamwise region flowing downstream from each wing tip and is classically referred to as the tip vortex. The detailed manner and mechanism of this process is not clearly understood but is commonly referred to as the "rolling up" of the trailing vorticity into the tip vortex. Clearly this process must include a radial inflow into the vortex in addition to rolling up (as a carpet) about it. Analyses which have

13

not accounted for radial inflow mechanism, such as Kaden's two-dimensional similarity solution, (Reference 1), usually predict unreasonably large vortex core diameters. Batchelor, using the Navier-Stokes equations (Reference 2), considers the axially symmetric vortex. He finds that contraction or expansion of the core (i. e. radial flow) and the axial acceleration or deceleration within it depends on whether the circulation of the vortex is increasing or decreasing. If the circulation of the vortex is increasing in the streamwise direction, there will be a corresponding falling of the pressure in the vortex core, a streamwise acceleration of the flow within it, and a radial inflow. Depending on the rate at which vorticity is transported to the core by the radial inflow, this process will accelerate, sustain itself, or decay. For the tip vortex, generated by a wing, this complex inter-dependent process will depend on the strength and strength distribution of the vorticity within the vortex sheet which is being ingested by the vortex; it will also depend on the relative amount of irrotational air being ingested from the field surrounding the forming vortex. The wing tip region thus has a significant influence on the formation and character of the tip vortex because it initiates the process and is the principle source of the vorticity entrained in it. This tip vortex formation process will be complicated further by the presence of components of vorticity other than trailing type, and by the state of the boundary layer, (i. e. whether it is laminar or turbulent). Because the vortex bursting phenomenon is associated with rapid axial decelerations in the vortex core region and these accelerations are apparently dependent on the rate of change of the vorticity in it, the possibility of inducing vortex bursting by proper design of the tip suggests itself. This could be a way of spreading the tip vortex and reducing its maximum induced velocities.

The discussion thus far has been concerned with the detailed mechanisms of the formation of the vortex wake of a wing. With respect to the goal of improving wing efficiency it is also helpful to consider the problem in a very gross (rather than detailed) manner. The following comments are based on momentum and energy considerations, and are concerned with the induced losses (i. e. induced drag and its associated energy).

The force generated by a wing is obtained by reacting against the body of air through which it passes. The lift, for example, is proportional to the rate at which net vertical momentum is being imparted to the body of air. Because momentum is proportional to the velocity and the energy to the velocity squared, it is always most efficient to create a given amount of momentum with the largest mass of air and the least induced velocity. Thus, the advantage of increasing the wing span (aspect ratio); it increases the extent of the wake, laterally. (It is noted that increasing the vertical extent of the wake would also improve the efficiency of the wing.)

Locally in the flow field, the momentum imparted to the flow is not necessarily downward. It can have horizontal components and even upward components (e. g. outboard of the tip vortices); the energy required to generate these components of momentum can be interpreted as lost since it is not directly associated with the lift. Thus, the efficiency of the wing will also be improved by reducing the magnitude of induced velocities in the flow

14

field which are not vertically downward.

The induced flow field is determined by the character of the vortex wake and this is in turn determined by the thin boundary layers of rotational air streaming from the region of the wing tips as discussed above. Because these boundary layers are strongly influenced by the wing tip geometry, there is a potential for improving the wing efficiency and/or favorably changing the character of the trailing vortices by proper design of the tip.

Aspect ratio is conventionally defined as the wing span squared over the wing area and is generally associated with the wing efficiency. Actually, it is the wing span rather than aspect ratio, per se, which influences the wing efficiency for a constant total lift (rather than constant C_L). This is evident by transforming the familiar expression for minimum induced drag coefficient

$$C_D = \frac{C_L^2}{\pi \, AR}$$

to dimensional form, ie.,

$$D = \frac{L^2}{\pi \, q \, b^2}$$

Thus the induced power required

$$P = DV = \frac{2 \, L^2}{\pi \, \rho \, V \, b^2}$$

is inversely proportional to the span squared. This is in agreement with the idea (from momentum and energy considerations) of extending the wake. For these reasons the total span of the wing was held constant for the various tip configurations tested in this investigation.

Visualization Results

The combined visualization of the flow field in the region of the wing tips with smoke in the external flow and oil on the surface provided an insight into the details of this highly three-dimensional flow region, especially with respect to the formation of the tip vortex. Although the changes in this flow field for the different tips tested were apparent, the results were only qualitative.

It should first be noted that considerable caution should be used when interpreting flow visualizations. A brief discussion regarding the interpretation of the flow visualizations is presented in Appendix B. Oil was used to visualize the surface (boundary layer) flow because it could be moved (and become streaked) by the surface shearing stresses. However, its motion was also simultaneously influenced by the surface pressure gradients and gravity. Because the wing was mounted vertically with the tip up for this investigation, gravity had a significant influence on the oil flow wherever the shear stresses became very small.

Caution must also be exercised when interpreting the smoke visualization. The smoke delineates streak lines (the path of the flow from a fixed point in it). When the flow is steady the streak lines are the same as streamlines which are everywhere parallel to the local flow velocity. However, it must be remembered that a photograph of these streamlines reveals only a two-dimensional projection of the local flow direction. That is, the component normal to the plane of the photograph is not apparent; this can be confusing in the highly three-dimensional-flow region of the wing tips. In the following discussions the term smoke filament is used only with reference to a visible streamline; a group of smoke filaments is referred to as a smoke stream or ribbon.

The flow visualizations are presented in Figures 7 through 22 and discussed relative to each other. In all the photographs the freestream flow is from left to right. The flow over the upper surface is visualized at the positive angles of attack. Because of the symmetric wing cross section, the same view at a negative angle of attack is a visualization of the lower surface flow at the corresponding positive angle of attack.

The following initial discussion is presented to aid the description of the interpretations of the smoke and oil visualization photographs. Figures 9 (a) and 11 (b) are typical examples of the oil surface flow and smoke flow photographs which were studied. Certain features of these photographs are referred to repeatedly. The association of these features with the interpreted characteristics of the flow is presented in Figure 7 in schematic form. The figure presents a perspective of the flow about the rounded-square tip configuration depicting the tip vortex and corresponding wing surface flow. Also presented are edge and top views of the perspective.

The edge view of Figure 7 shows the tip vortex (in a crossflow plane) as formed over the wing at a slightly inboard position. The vortex is shown as being formed primarily from the boundary layer on the lower surface. Upper surface boundary layer fluid is also drawn into the vortex from the region outboard of the attachment point (a line in the planview). The attachment line is formed by the flow, induced by the vortex, impinging on the wing surface; it appears as a stagnation point in this crossflow plane. The flow outboard of the attachment line in the boundary layer is depicted as having an outward spanwise component of velocity while that on the inboard side is shown having an inboard component. (Keep in mind the downstream velocity components due to the freestream are also present although not shown in this view.) The upper surface boundary layer air flowing outboard encounters an adverse spanwise pressure gradient and eventually separates and is drawn into the vortex as shown. The spanwise component of the lower surface boundary layer flow also encounters an adverse pressure gradient and separates along some line on the lateral edge of the wing (shown in the figure arbitrarily as the chord plane). These upper and lower surface boundary layers provide the rotational air which sustains the tip vortex. In addition to the boundary layer air some freestream

16

air is ingested directly into the vortex. Other portions of the freestream air are induced to flow about the vortex in a resultant helical path.

Thus, a smoke filament deposited in the flow upstream of the wing might be expected to follow one of several paths depending upon its location relative to the wing tip. If it were a dividing streamline, the smoke filament would end up in the boundary layer flow and hence in the vortex core. If it were slightly displaced from the dividing streamline, it might be expected to be in that portion of the freestream which is ingested directly into the vortex in the immediate vicinity of the tip. A filament even further displaced, would be expected to move downstream about the vortex and describe a helical path. Indications are that the closer to the center of the vortex the filament is, the greater the pitch of the helix becomes. The perspective in Figure 7 attempts to portray the appearance of two ribbons of smoke, external to the boundary layer, being affected by the vortex. The following interpretations of the photographs taken of the smoke visualization studies confirm the general features of the model described above.

The behavior of the flow at the juncture of the boundary layer and the wing surface was visualized by the oil flow studies and is typified by the top view of the wing tip in Figure 7. The shape and direction of the oil path lines are indicated by the arrowed lines emanating from the attachment line. The attachment line is characterized by oil paths which appear to move away from a common line or envelope. The separation line is characterized by oil paths which appear to move toward a common line. Since the separation region is characterized by an adverse pressure gradient, the oil tends to collect in this area. These features of the surface oil flow have been emphasized and noted on the photograph of Figure 9 (d) which is a duplicate of that in Figure 9 (a). (Note: The two white dots on the lower portion of the wing are simply the fasteners for the replaceable wing tips.)

Due to the relatively low Reynolds number of these tests, difficulties with laminar flow separation were anticipated and it was thought that they could be avoided by the use of boundary layer trips. However, attempts to do so were not successful. A sequence of surface flow visualizations which demonstrate the variations encountered in the wing boundary layer flow pattern with angle of attack is shown in Figure 8. Because of the magnitude and chordwise extent of the favorable (negative) pressure gradient over the forward part of this airfoil (NACA 0012) at low angles of attack and the operating Reynolds number (about 190,000), the boundary layer trip was not able to fix the laminar to turbulent transition to a forward location. Transition was thus occurring farther back on the airfoil and in the same chordwise region as the laminar separation; this made the flow extremely sensitive to small shifts in the relative location of transition.

The laminar boundary layer decelerates under the action of the adverse (positive) pressure gradient which exists over the aft section of the airfoil. If this adverse pressure gradient (which depends on angle of attack) is sufficient, the laminar layer will separate before transition to the turbulent state. Transition of this laminar boundary layer after separation can cause it to reattach forming a separation bubble as observed at α = -2 degrees in Figure 9. Here the separation is evidenced by the downward turning of the oil streak to a vertical asymptote at the line of separation as the streamwise (horizontal in photos) shear force diminishes to zero at the separation line. For a short distance beyond the separation line, the oil runs vertically down the wing due to gravity. The chordwise extent of this separation region of running oil ends abruptly at the reattachment line which is evidenced by the forward edge of the area scrubbed relatively clean of oil by the high shear forces of the turbulent reattaching boundary layer. An example of transition of the boundary layer from laminar to turbulent before separation is observed at α = +1 degree in Figure 8. Here the oil streaks which begin turning downward, due to the diminishing shear force, are observed to straighten out abruptly at the location of transition due to the increased streamwise shear.

At an angle of attack of about 8 degrees, a leading-edge separation bubble would usually form and persist up to stall; this is observed in Figure 9 at α = +10 degrees as a collection of oil along a narrow strip at the leading edge.

Rounded-square tip.- The flow visualizations for the rounded-square tip configuration are presented in Figures 9 to 12. The surface flow patterns in the vicinity of the tip are shown in Figure 9 and smoke flow about it in Figure 10. Additional smoke flow visualizations presented in Figures 11 and 12 are intended to show the details of the tip vortex forming about this tip.

For the wing at α = -10 degrees (which represents the lower surface of the wing), the surface oil flow pattern is presented in Figure 9 (b). This pattern indicates that the lower surface flow near the tip is outward and around the lateral edge of the tip. In (a) for α = +10 degrees there is evidence of an attachment line and a separation line. Between them the oil flow is outward from the attachment line to the separation line. The locations of the lines are noted in (d) which is the same photograph. Just inboard and adjacent to the separation line there is a very narrow chordwise oriented region where the direction of the outward oil flow is virtually normal to the separation line. This is indicated in (d) as a region of dots. These observed features of the surface oil flow pattern are all evidence of the vortex forming over the upper surface of the tip as can be observed in the smoke visualizations of Figures 10 to 12. As the lower surface boundary layer flow (vortex sheet) from the lower surface attempts to follow the surface around the tip, it separates from the surface along what is referred to as the primary separation line. This is the outboard separation line indicated in Figure 7. This separated sheet of vorticity rolls-up into a vortex above the tip

18

near its outboard edge. Due to the flow field about this vortex forming above the tip, there is a component of the flow impinging on the surface inboard of the vortex. On the surface this impinging flow separates into regions of inward and outward flow components at the attachment line. The outward flow passes under the vortex (as noted in (d)) and separates at the secondary separation line. (This is the same phenomenon which occurs over the leading edges of low-aspect-ratio delta wings and has been reported and described many times in that literature, e.g., References 4 and 5.)

The surface flow pattern for α = 0 degrees is presented in photograph (c) of Figure 9 as a reference. Comparisons of (a) and (c) indicate the changes due to angle of attack. It is noted that at α = 0 degrees there is an inward turning of the flow near the tip which reflects the thickness pressure distribution and its spanwise gradient.

A sequence of photographs of the smoke visualization about the rounded-square tip configuration is presented in Figure 10; photographs (a) - (e) are for α = +9 degrees, (f) - (k) are for α = -9 degrees, and Figure 10(l) is for α = -5 degrees. Photographs (a) and (f) are partial front views at α = +9 degrees and α = -9 degrees, respectively, in which the wake can be seen farther downstream than in the other views. The photographs following (a) and (f) are arranged so that in each succeeding picture the particular smoke stream passing around the tip is observed to become entrained in the tip vortex at locations which are successively farther downstream.

The smoke flow visualization substantiates the general description of the formation of the tip vortex over the tip which was presented above. For example, the trailing vortex core can be traced forward over the same narrow region of outboard flow noted in Figure 9 (d). The flow around the tip from the lower to the upper surface and its entrainment into the vortex forming over the upper surface is clearly evident (see, e.g., Figure 10 (i)).

For comparable conditions, the visualization of the tip vortex generated by the rounded-square tip configuration was the most clearly defined of all tips tested, and it presented the appearance of being the most concentrated. This clear definition is evident in each of the visualizations of Figure 10. It is also observed (e.g., in (c)) that the spanwise contraction of the wake (i.e., the inward displacement with streamwise distance) appears relatively slight. A comparison of photographs (j) and (l) (α = -9 degrees and -5 degrees, respectively) indicates that the character of the flow does not change with angle of attack.

More detailed visualizations of the tip vortex formation.- The details of the formation of the tip vortex on and about the rounded-square tip can be observed in the smoke flow photographs presented in Figures 11 and 12. The results in Figure 11 are for a freestream velocity of about 60 fps. and those in Figure 12 were obtained at about 15 fps. The results at

60 fps. were obtained before the boundary-layer trips were installed. In each figure the sequence of photographs is arranged in an order which shows the smoke entering the vortex at progressively farther downstream locations. In studying these visualizations it should be remembered that all the photographs within each figure are of the same flow. The only difference is in where the smoke has entered the flow and thus each photograph is a visualization of different parts of this flow. Furthermore, it should be remembered that the relative positions of the smoke filaments with respect to the plane of viewing is not always evident.

It is first noted that the flow pattern about the tip at 60 fps. (Figure 11) appears to be practically identical with that at 100 fps. (Figure 10). The only noticeable difference is that at 100 fps. the vortex is not as well defined (e.g., compare Figures 10 (b) and 11 (b)). This is attributed to differences in the turbulence level of the rotational air of the vortex in the two cases. At 100 fps., with the trip, there is more turbulence than at 60 fps. without the trip. Thus, the greater mixing at the higher turbulence level destroys the laminar appearance of the entrained smoke stream. At 15 fps. (Figure 12) the tip pattern appears similar to that at the higher velocities except for the persistence of the laminar flow appearance in the vortex farther downstream.

In Figure 11, the inner part of the vortex forming over the upper surface of the tip has been made visible by the smoke and can be seen in photographs (a) - (d), especially in (d) which is a lighter print of (c). The visualized part of the forming vortex can be faintly observed as far forward as about 15 percent of the chord (the region of the glare of light from the tip). The entrainment of irrotational air from various parts of the flow field into the forming vortex is evident by examining the sequence of photographs in Figure 11. The radial inflow associated with the concentration and rolling up of the trailing vorticity is especially evident in Figures 11 (i) and (l). In (i) the bright ribbon of smoke passing around the tip is observed to become entrained into the vortex. The same is seen in (l) only farther downstream.

At a freestream velocity of about 15 fps., a more detailed view of the structure of the forming tip vortex is seen in the photographs of Figure 12. However, because the inboard portion of the wing was stalled at this angle of attack (α = +9 degrees), only the initial part (downstream to about one chord length from the trailing edge) of the flow pattern may be representative. In photograph (b) the smoke stream is initially of a ribbon-like form (with a relatively flat cross section) as it passes around the wing tip and over the forming vortex. If it is followed, it is observed that the smoke filaments on the upstream edge of this ribbon-like smoke stream lead into the central part of the vortex while those on the downstream side lead to the outer parts of the vortex. The stream distorts quite rapidly; however, its cross section is still discernable after it has made one turn around the vortex. Here, coming out of the viewing plane, its cross section appears to have doubled its streamwise dimension. It also appears to have its upstream half deflected

inward toward the center of the vortex as if the cross section were bent. In photographs (c) and (d), where the smoke streams appear to be composed of multiple ribbons, distortions similar to those in (b) are observed.

The blunt-square tip.- The surface oil flow and smoke visualizations for the blunt-square tip are presented in Figures 13 and 14, respectively. The surface flow pattern in the region of the tip at α = +10 degrees and α = -10 degrees (Figure 13 (a) and (b) appear to be generally similar to those of the rounded-square tip (Figure 9). However, at α = +10 degrees it can be seen that the area on the upper surface between the secondary separation line and the lateral edge of the tip is greater for the blunt-square tip than for the rounded-square tip (Figure 9). It is further noted that the primary separation line must be at the sharp edge of the lower surface at the tip. Thus, there is apparently a larger region of separated flow about the blunt-square tip than the rounded-square tip which will become entrained in the forming vortex. This could result in more mixing and thus explain the slightly more diffuse (relative to rounded-square tip) appearance of the forming vortex which was observed during the smoke visualizations of this tip. The leading-edge separation bubble (which was present on all the wing configurations at the higher angles of attack) is clearly observed at α = +10 degrees as the narrow region of oil accumulation along the leading edge. The surface flow pattern at α = 0 degrees which is due to the wing thickness pressure distribution is presented in (c) of Figure 13. There appears to be evidence of a weak trailing vortex forming very close to the lateral edge over the aft part of the tip due to the separation of the inward flow off the flat end surface of the tip (at the sharp edge). This must occur on both the upper and lower surfaces so that the net trailing vorticity is zero.

The smoke flow photographs of Figure 14 also display the general similarity of the flow pattern about the blunt-square tip with that about the rounded-square tip. Photograph (a) is a partial front view showing the downstream portion of the wake in which the relatively concentrated tip vortex can be observed. The view in (b) is outward and upstream from a point slightly behind the wing and shows the flow outboard and around the tip (near the trailing edge) becoming entrained into the vortex as it proceeds downstream. The relatively slight spanwise contraction of the wake for this tip can be observed in (c) (at the right edge of the photograph).

The 45-degree swept-forward tip. - The flow visualizations, for the 45-degree, swept-forward tip configuration, are presented in Figures 15 and 16. At α = +9 degrees in Figure 15 (a), the oil streaks are observed to be sharply turned inward so that they appear to become asymtotic to the tip trailing edge. Because the oil appears to be experiencing high shear, the effects of gravity are not believed to be dominant with respect to this inward turning of the oil on the upper surface. At α = -9 degrees in (b) the oil streaks are observed to be turned outward slightly. The smoke photographs (c) and (d) of Figure 16 indicate that most of the inward turning of the flow at the upper surface (observed as a fanning of the smoke stream approaching the trailing edge) has occurred through the boundary layer on the upper

surface due to the strong spanwise pressure gradients. Thus, the net
change in direction of the flow across the sheet of trailing vorticity is less
than would be deduced from the surface flow patterns. For α = +9 degrees,
the surface flow pattern at the outermost extremity of the wing, just aft of
the leading edge grit, is seen to be outboard and virtually normal to the
swept trailing edge over a small area. This area is just inboard of the
vortex observed to be streaming aft and inward from the apex of this tip
in the smoke photograph of Figure 16 (a). (The vortex is more easily dis-
cerned by viewing the photograph at a very shallow angle to its surface and
in the streamwise direction). In Figure 15 (b) at α = -9 degrees, the
bright narrow region of oil along the leading edge near the tip which becomes
faint inboard is believed to be the stagnation region. It is not clear why the
oil accumulation becomes greater near the tip; possibly it is due to a rela-
tively strong spanwise pressure gradient in that region.

During the smoke visualization of the flow about the 45-degree,
swept-forward tip, it was much more difficult to obtain a visualization of
its forming vortex than it was for the two square planform tips. When
smoke was entrained into the streamwise region of concentrating vorticity,
the vortex had the appearance of being relatively more diffuse as can be
observed in photographs (a) and (b) of Figure 16. The spanwise contraction
of wake is observed in (a) to be relatively large. For this configuration,
substantially all the vorticity (the rotational boundary layer air from the
two surfaces) must separate from the wing along the trailing edge. Thus,
the concentrated trailing vortex will form only by the rolling up of this
essentially flap sheet of vorticity in the wake behind the wing. On the square
tip planform configurations, however, a substantial amount of the total
vorticity separates from the wing along the lateral edge. This initial con-
figuration of the separated vortex sheet facilitates the rolling up over the
surface of the tip.

The 60-degree, swept-forward tip . - The flow visualizations for
the 60-degree, swept-forward tip, presented in Figures 17 and 18 are
observed to be generally similar to those for the 45-degree, swept-forward
tip. However, the following small differences of the flow about the 60-degree
tip relative to that about the 45-degree tip are noted. In Figure 17 at α = -10
degrees there is more outward turning of the surface flow pattern indicating
a stronger spanwise pressure gradient. At α = +10 degrees, over the
downstream half of the swept trailing edge of the tip, the flow pattern appears
to be inboard from the edge; this would imply a flow around the edge from the
lower surface (at least within the boundary layer). The forming vortex was
actually more clearly discernable than the photograph of Figure 18 would
indicate. The spanwise contraction of the wake is greater than was observed
for the square tips and comparable to that of the 45-degree, swept-forward
tip.

The 45-degree, swept-aft tip. - The surface oil flow and smoke
flow visualizations for the 45-degree, swept-aft tip are presented in Figures
19 and 20, respectively. Along the swept leading edge, at α = +10 degrees
in Figure 19, there is observed a narrow region of accumulated oil due to a

leading-edge separation bubble. About midway along the swept leading edge, this narrow region of accumulated oil is observed to become considerably wider; aft and outward from this region the surface oil flow has a swirl pattern of increasing radius. These observed features are characteristic of flow over swept wings (e.g., see Reference 6, pages 166-170) and low-aspect-ratio delta wings.

In photograph (c) for α = +6 degrees similar features are observed except they are confined to a smaller region at the outer end of the tip and thus the swirl pattern is virtually eliminated. This flow pattern on the swept-aft tip is due to the separation of the lower surface boundary layer (sheet vorticity) as it moves outward and around the tip leading edge. Over the inboard part of the tip leading edge it reattaches to form a leading-edge bubble. Farther out on the tip the character of the flow changes such that it rolls up over the surface to form a vortex. The similarity of this vortex formation process with that for the square tips should be recognized; the fundamental difference is in the sweep angle of the primary separation line.

In general, the trailing vortex behind the 45-degree, swept-aft tip appeared relatively diffuse as is observed in the smoke photographs of Figure 20. The spanwise contraction of the wake was judged to be comparable to that of the 45-degree and 60-degree, swept-forward tips. In photograph (c) which is for α = -10 degrees, most of the smoke stream on the far side of the wing is on the far side of the forming vortex and thus is moving inboard (the bright inboard sloping stream). A part of it, however, has passed on the near side of the vortex, has become entrained in the sheet of vorticity and has an outward velocity component; this is observed as the faint outward fanning of the smoke from the bright inboard sloping stream, especially at the trailing edge. Photographs (a) and (b) show the entrainment of the irrotational smoke stream into the trailing vortex sheet and the forming vortex.

The cusp tip. - The surface oil flow and smoke flow visualizations for the cusp tip are presented in Figures 21 and 22, respectively. The objective of the cusp-like planform was to approximate a spanwise loading gradient of zero at the tip and thereby generate a trailing vortex sheet whose strength approached zero at its outboard edge. The surface flow patterns for this tip are quite similar to those of the 60-degree, swept-forward tip (Figure 17). The surface flow pattern on the upper surface of the narrow portion of the tip was always sharply inward while on the lower surface it was almost streamwise. The forming vortex appeared diffuse (Figure 22) but no more so than for the other swept tips. It is noted, especially in (c), that the forming vortex appears to be originating from the highly swept part of the trailing edge, just as if the outer portion of the tip were not present. Because of this, the forming vortex is much farther inboard relative to the span of the wing, than for the other tip configurations. This configuration, therefore, has the smallest "effective span" and might be expected to be the least efficient.

23

As a result of the visualizations, it has been deduced that the square-planform tips apparently aid the concentration of the trailing vorticity into the tip vortex by shedding much of this vorticity as a sheet along the streamwise oriented edge. This vortex sheet rolls up over the tip into a concentrated vortex and, therefore, the forming tip vortex is close to and parallel to the source of vorticity from the streamwise oriented edge. The rate of increase of the circulation along the axis of the forming vortex is believed to be greater for the square tips than for the other tips. This is believed due to the relative orientation and proximity of the vortex and the source of vorticity. This greater rate of increase of circulation would, for a given axial location in the vortex, result in greater circulation, a faster rolling up (coiling) of the sheet, and a larger radial inflow. The faster roll up of the sheet of vorticity due to the larger circulation would provide more coils of vorticity. The greater rate of increase of the circulation along the vortex axis would result in a greater radial inflow of this vorticity to the vortex and, thus, a more concentrated vortex (as shown by Batchelor, Reference 2, and described in the general discussion).

It was also noted that the square-tip wing generated a tip vortex whose spanwise location in the wake was farther outboard than that of the other tips.

Force Measurement Results

The results of the balance measurements, obtained for the six tip configurations are presented in Figures 23 through 34. These results are in the form of wing polars (lift coefficient (C_L) versus drag coefficient (C_D)) with the pertinent information relative to wing area, test section dynamic pressure and wall suction noted on each figure.

As noted previously, one of the objectives of this program was to determine the effect of various tip geometries on the performance (i. e. , lift versus drag) of a wing. This objective was not realized due to the sensitivity of the wing forces to relatively small changes in the pressure distribution which arose from the unpredictable changes in the wing boundary layer flow (discussed and illustrated in the previous section on the flow visualizations). This problem, due to the low Reynolds number of the tests (about 190, 000), was anticipated and it was thought that it could be avoided by the use of a boundary layer trip. However, for this airfoil and Reynolds number, attempts to develop a boundary layer trip which was effective simultaneously on both surfaces and over the entire angle of attack range of the tests were not successful.

These force data should not be relied on to assess the influence of wing tip design on the wing forces. Although the value of the measured force results has been discounted, they are presented and discussed to illustrate

24

the nature and magnitude of the effect of this problem on the measured wing forces.

Figures 23, 24, and 25 (Runs 1, 2, and 3) present the C_D versus C_L results of three runs for the rounded-square tip configuration. The circled points represent the data taken as the magnitude of the angle of attack was increased and the squares represent the data taken as the angle of attack was returned to zero. For all three runs, the tunnel dynamic pressure (q) was nominally 0.1 psi and the wall suction level was set at 50 mm of alcohol. Runs 2 and 3 were made several days after Run 1 and in the interim the tip had been removed and visualization and force tests made with several other tips.

The results of Run 1 (Figure 23) are observed to be noticeably different from those of Runs 2 and 3 which are nominally the same. This noted difference exceeds the estimated experimental errors associated with C_L and C_D. Since there was no observed change in either the model geometry or the test section flow conditions, it is believed that these differences in the results were due to changes in the boundary layer flow on the wing and that these changes were not consistently repeatable. Further support for this supposition is presented below.

Figure 26 shows the effect on the wing polar of a 10 percent increase in tunnel dynamic pressure obtained for the rounded square tip configuration. The variation of C_L with C_D and the value of C_D at $\alpha = 0$, obtained at this higher q are in closer agreement with the results of Runs 2 and 3 (Figures 24 and 25) than those of Run 1 (Figure 23). While the agreement with Runs 2 and 3 is reasonably good for positive values of C_L, it is not as good at the negative values where the C_D is observed to be slightly less than obtained in Runs 2 and 3 but it is not as low as obtained in Run 1 (Figure 23).

Figures 27 and 28 present the results for the swept forward 45-degree tip configuration obtained at two different wall suction levels; the results in Figure 27 were obtained with the wall vacuum set at 50 mm of alcohol and those in Figure 28 with it set at 30 mm of alcohol. The effect of increasing the vacuum is pronounced. The wing polar has moved to lower values of C_D when the vacuum was increased. Also, the shape becomes more parabolic and the peculiar behavior for the range of negative C_L disappears. It was hypothesized that at the lower vacuum levels, a vortex could form at the wing root-wall juncture, thereby effectively reducing the aspect ratio of the wing. This would explain the shift to higher drag values at a given C_L when the vacuum was reduced. However, it does not explain larger C_D at $C_L = 0$ or the asymmetry of the wing polar in Figure 28, nor does it explain the sharp dip in C_D at $C_L = 0.25$, nor the apparent hysteresis effects observed for increasing and decreasing wing angle of attack. These are more likely the result of changes in the character of the boundary layer flow. Hence, the information in Figures 27 and 28 was interpreted as further substantiation of the fact that the character of the boundary layer flow could change markedly at these Reynolds numbers.

46

FREESTREAM
VELOCITY

WING

VORTEX

ATTACHMENT
LINE

SEPARATION LINES

PICTORIAL OF FLOW ABOUT FORMING
TIP VORTEX AND CORRESPONDING SURFACE FLOW

ATTACHMENT
LINE

SEPARATION
LINES

REGION OF
OUTWARD FLOW
UNDER VORTEX

TOP VIEW OF WING TIP

VORTEX

ATTACHMENT
POINT

WING

SEPARATION
POINTS

EDGE VIEW LOOKING UPSTREAM
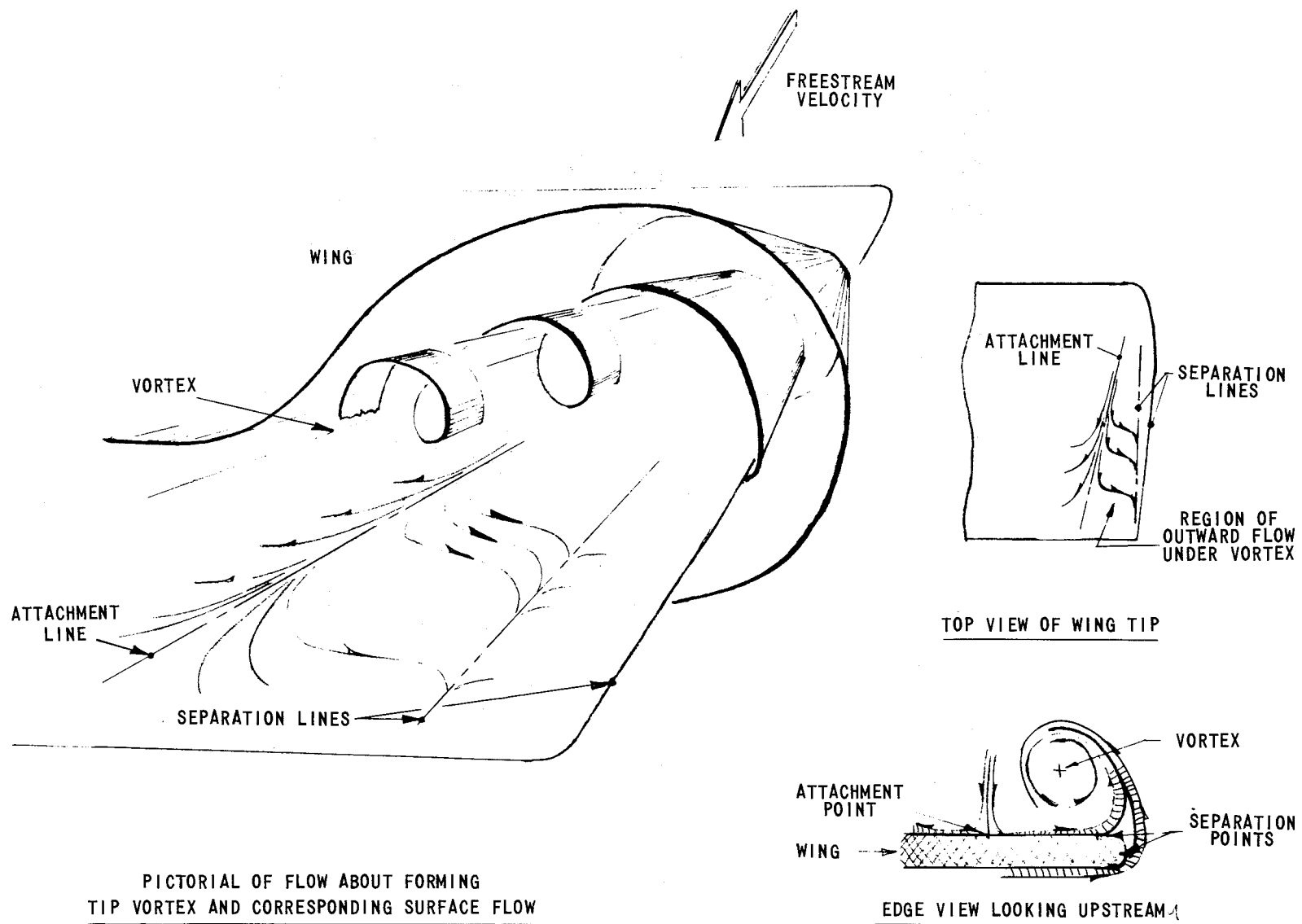
Figure 7. SKETCHES OF TIP FLOW PATTERNS

$\alpha = 0°$ $\alpha = +1°$ $\alpha = +2°$ $\alpha = +4°$ $\alpha = +6°$ $\alpha = +10°$

NOTE: FREE STREAM DIRECTION IS FROM LEFT TO RIGHT

$\alpha = -1°$ $\alpha = -2°$ $\alpha = -4°$ $\alpha = -6°$ $\alpha = -10°$
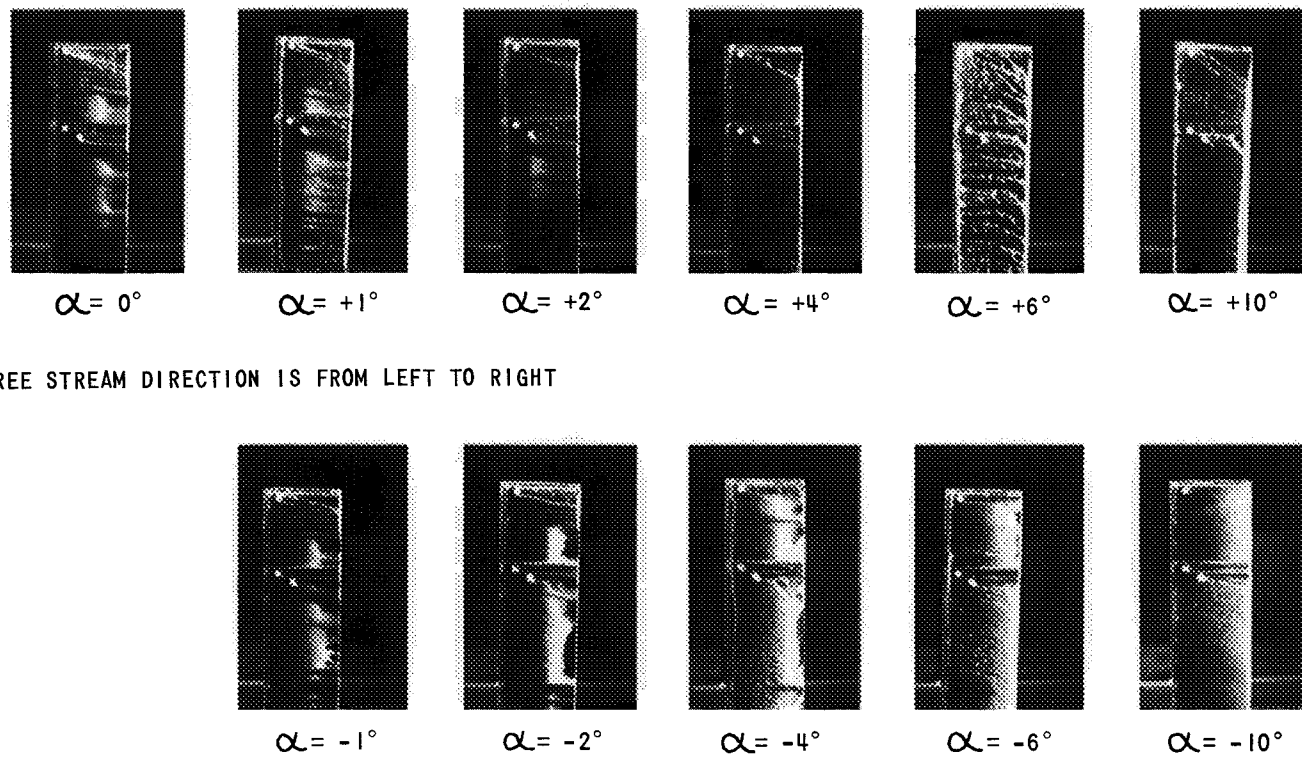
Figure 8.   TYPICAL OIL SURFACE FLOW PATTERNS OVER THE ANGLE OF ATTACK RANGE
FROM $\alpha = +10°$ TO $\alpha = -10°$; $V \approx 115$ fps
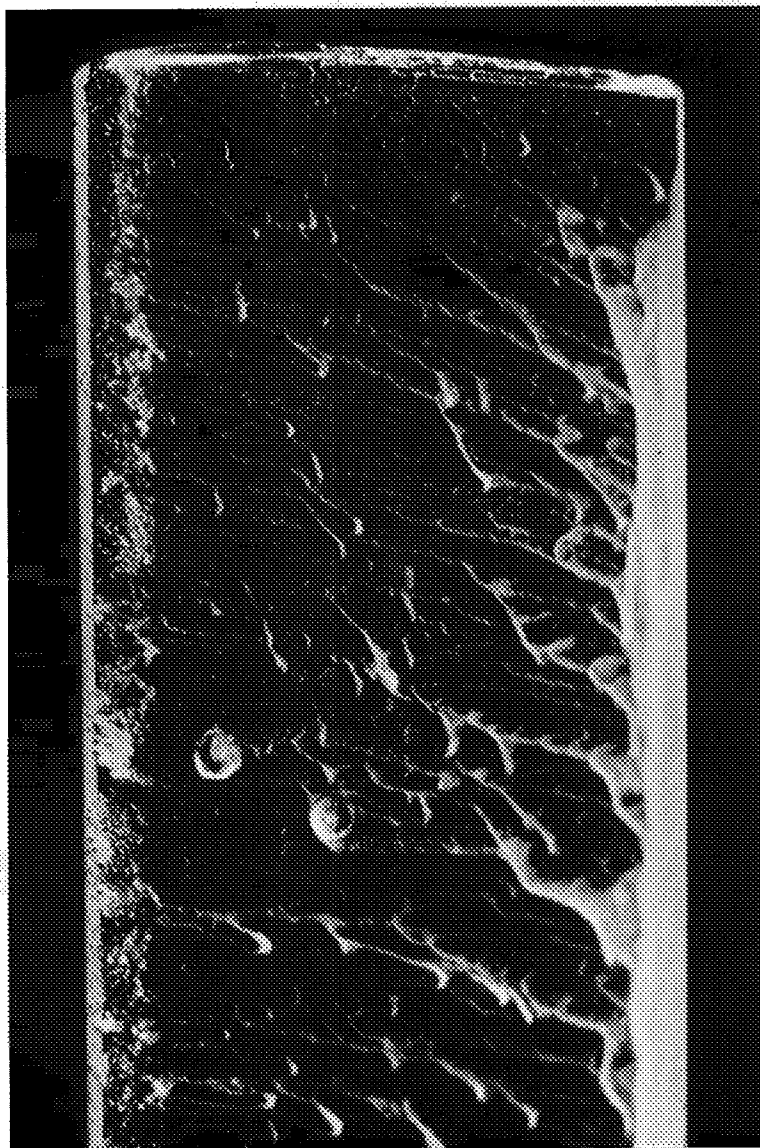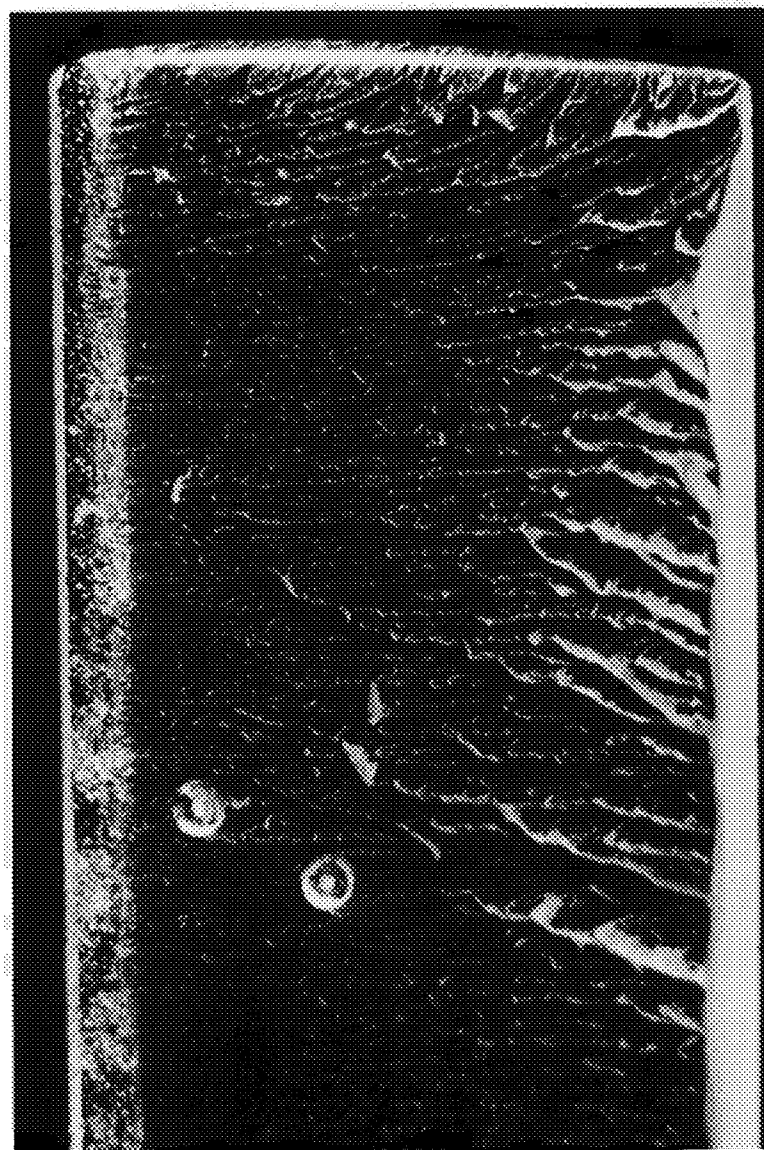
(a) $\alpha = +10°$ (b) $\alpha = -10°$

Figure 9. SURFACE OIL FLOW PATTERN ON ROUNDED SQUARE TIP; $V \approx 115$ fps
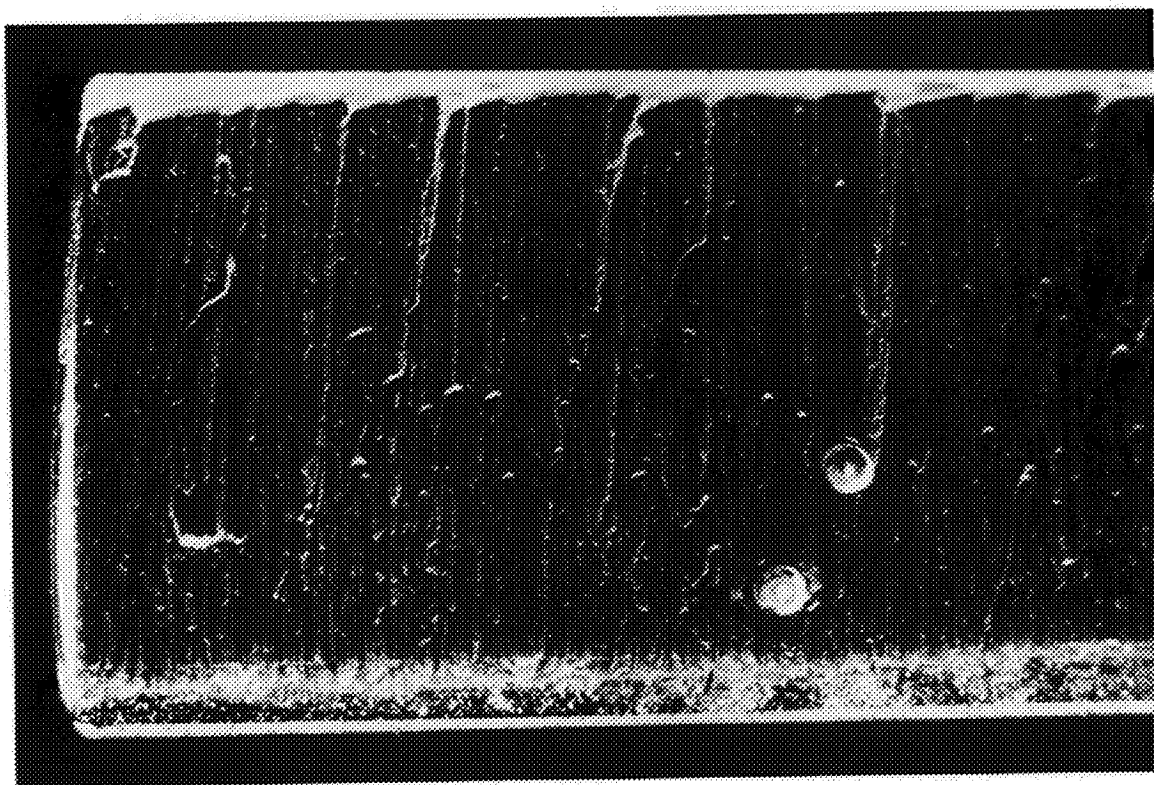
(c) $\alpha = 0°$

Figure 9. (Continued)
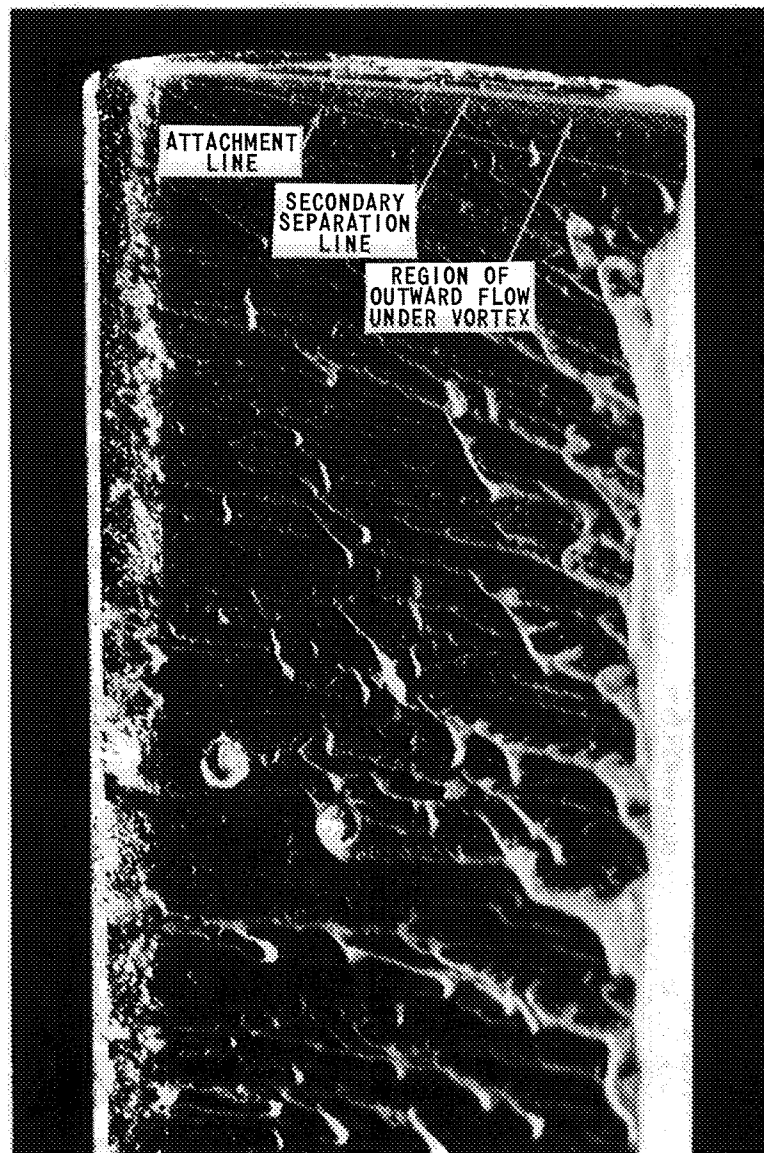
(d) α = +10°

Figure 9. (Continued)

$\alpha = +9°$ (a)

$\alpha = +9°$ (b)

$\alpha = +9°$ (c)
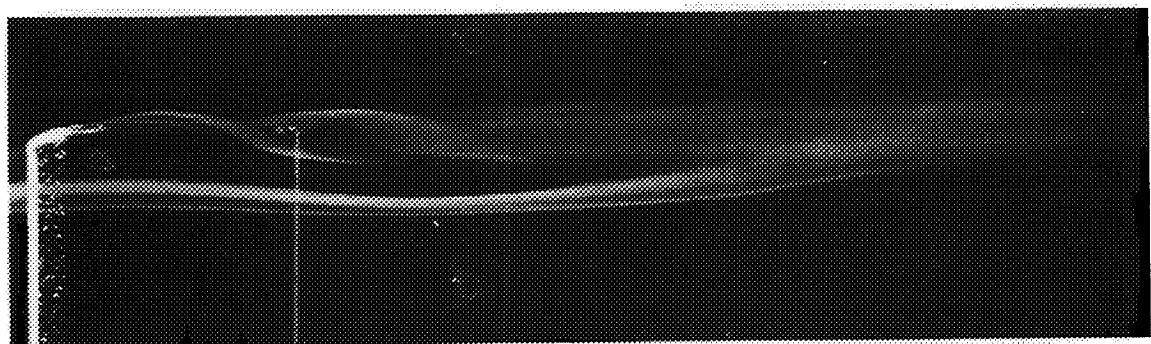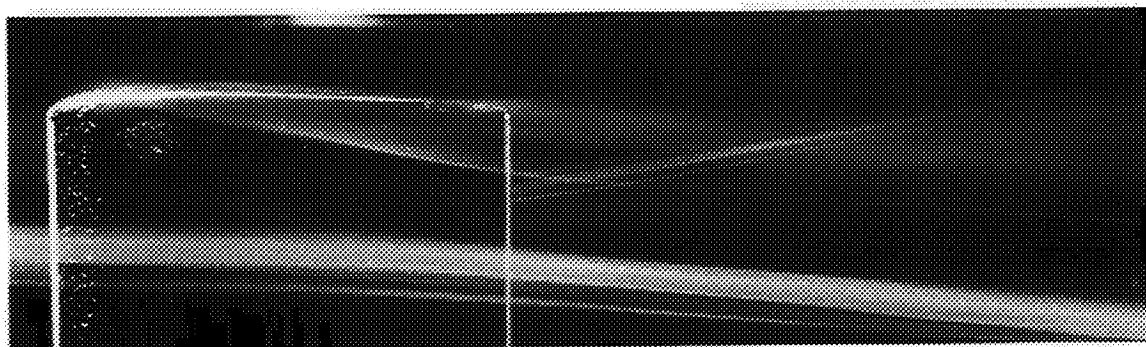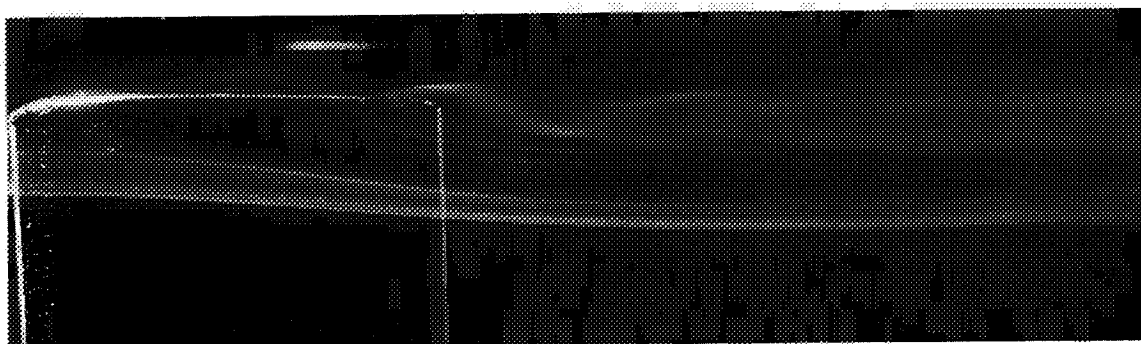
Figure 10. SMOKE FLOW ABOUT ROUNDED SQUARE TIP; $V \approx 100$ fps

$\alpha = +9°$

(d)

$\alpha = +9°$

(e)

$\alpha = -9°$

(f)

Figure 10. (Continued)

52

$\alpha = -9°$

(g)

$\alpha = -9°$

(h)

$\alpha = -9°$

(i)

Figure 10. (Continued)

$\alpha = -9°$ (j)

$\alpha = -9°$ (k)

$\alpha = -5°$ (l)
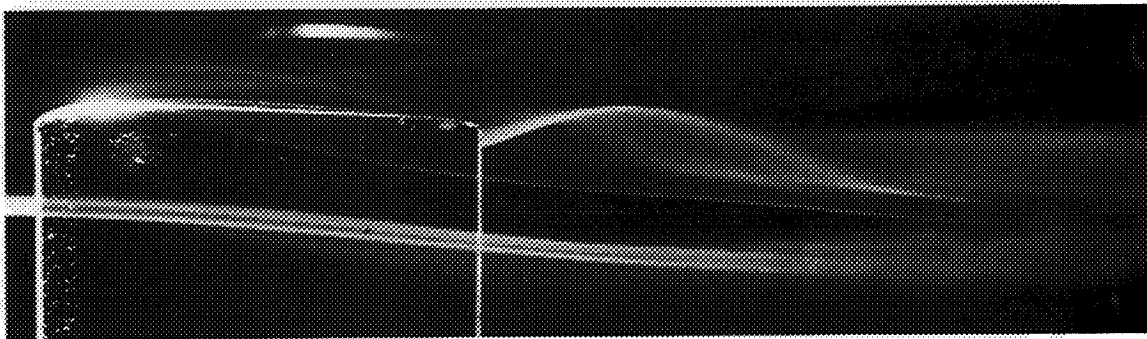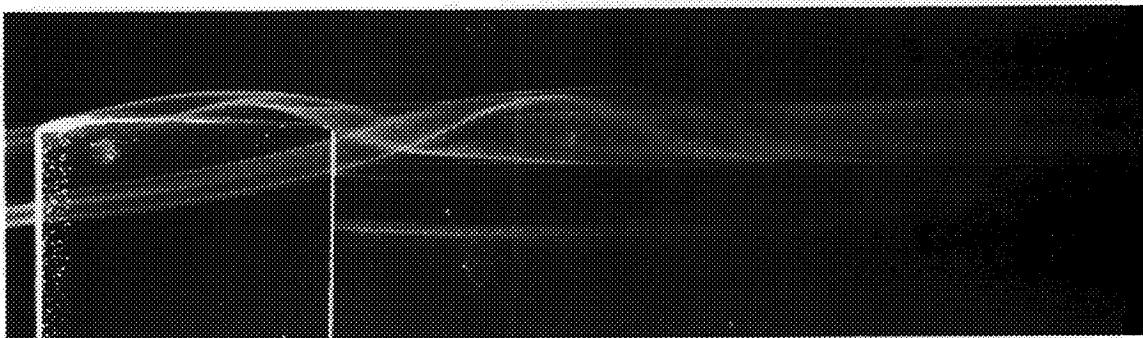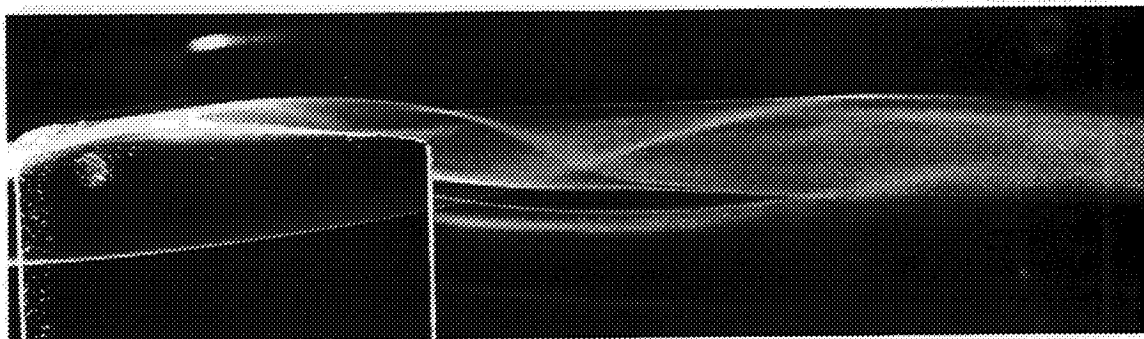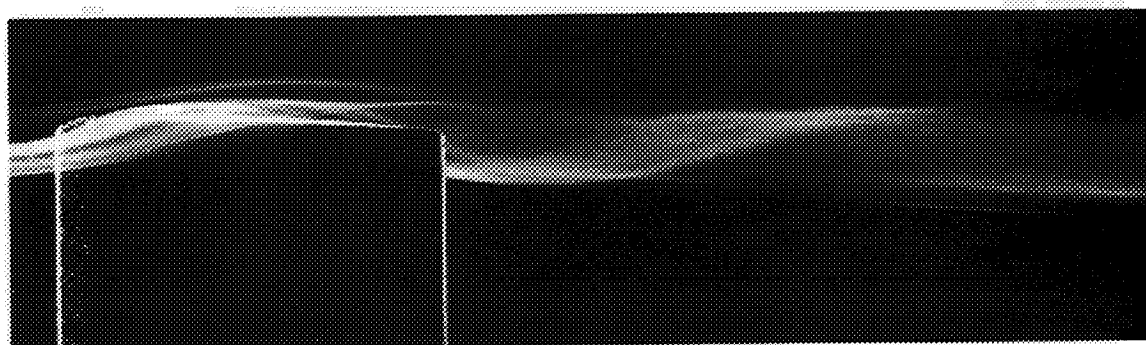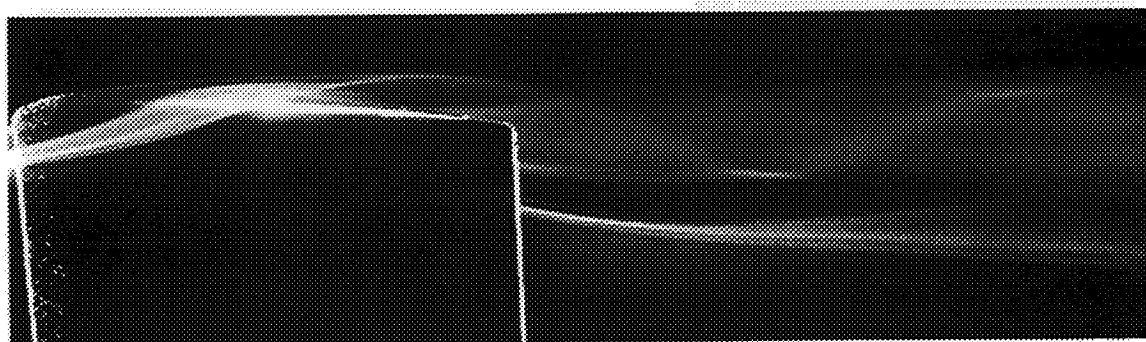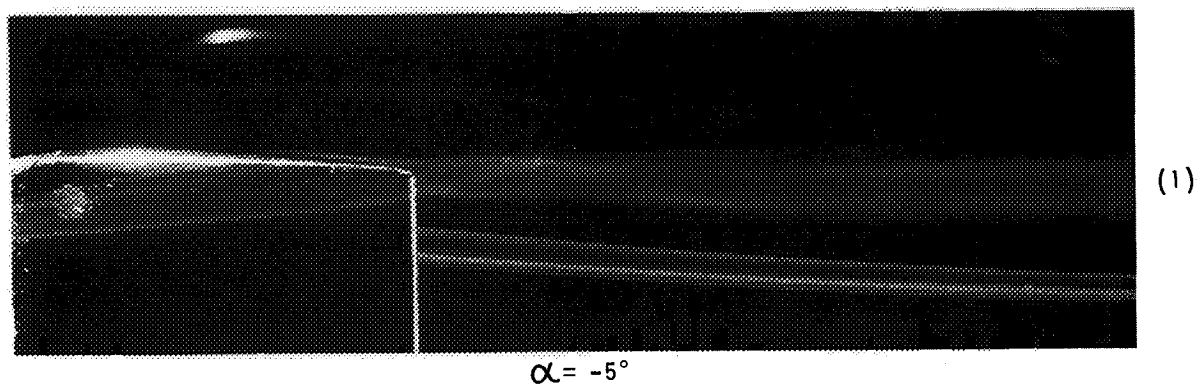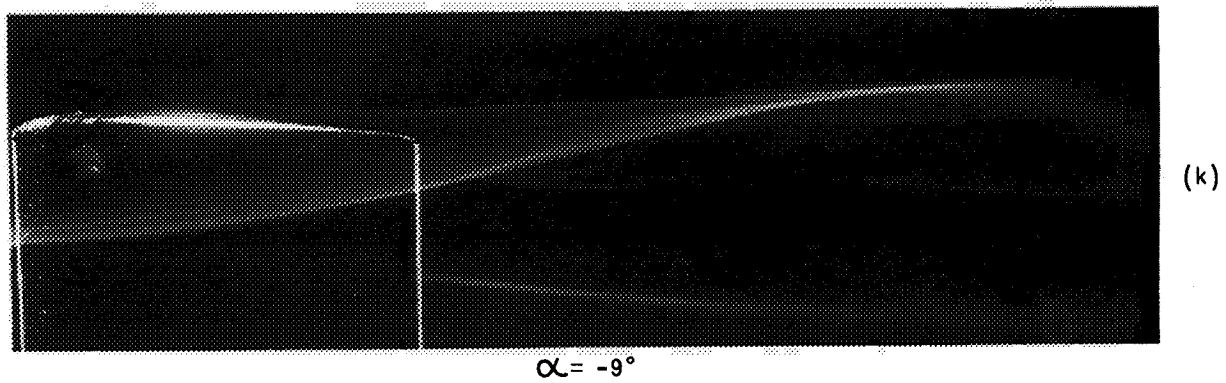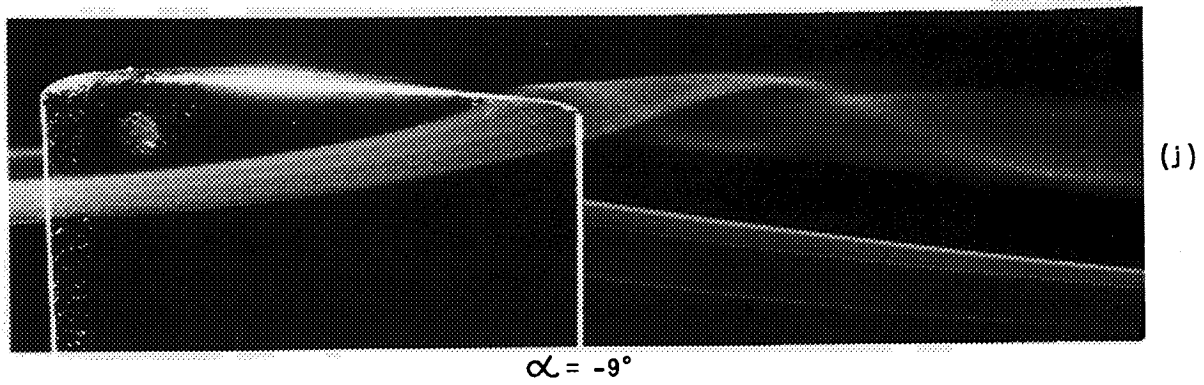
Figure 10. (Continued)
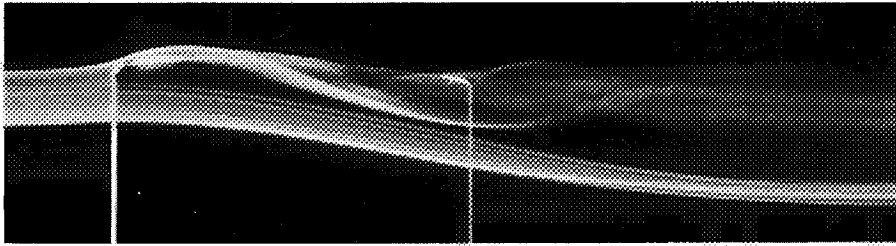
(a)
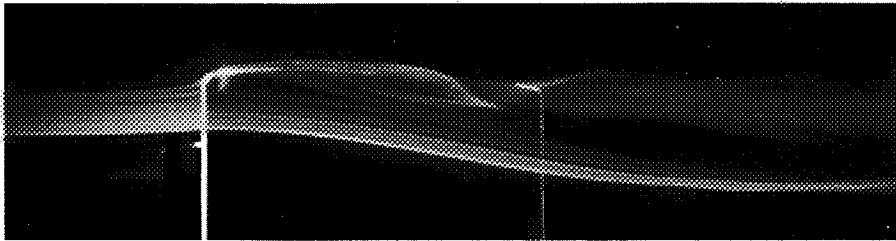
(b)
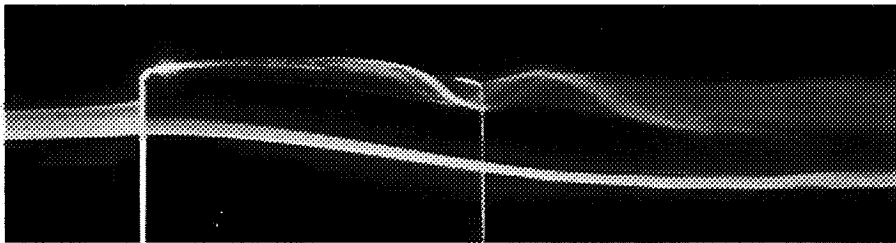
(c)
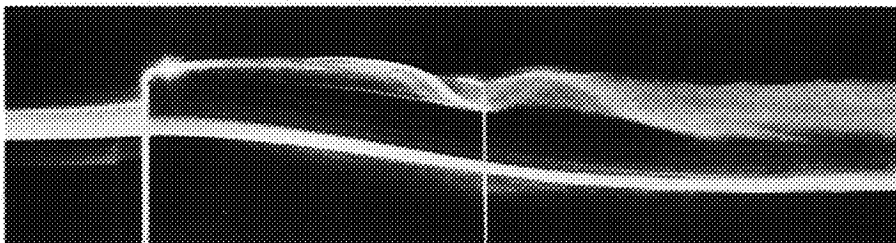
(d)

Figure 11. SERIES OF PHOTOGRAPHS SHOWING DETAILS OF THE TIP VORTEX
STRUCTURE; $V \approx 60$ fps, $\alpha = +10°$
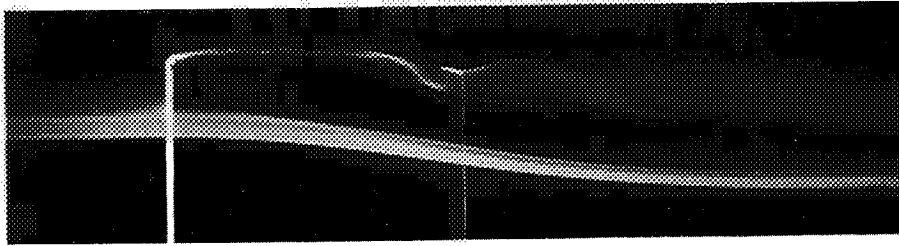
(e)
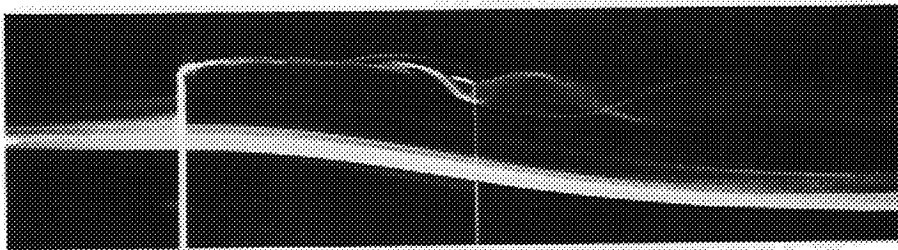
(f)
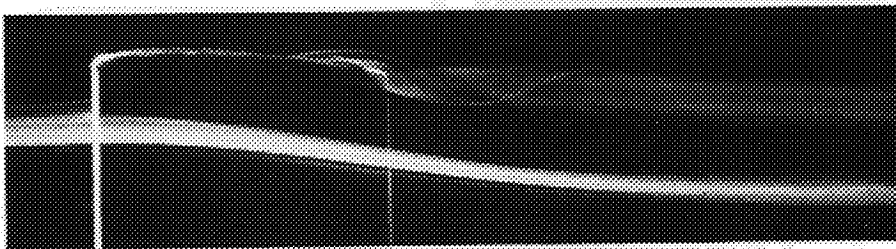
(g)
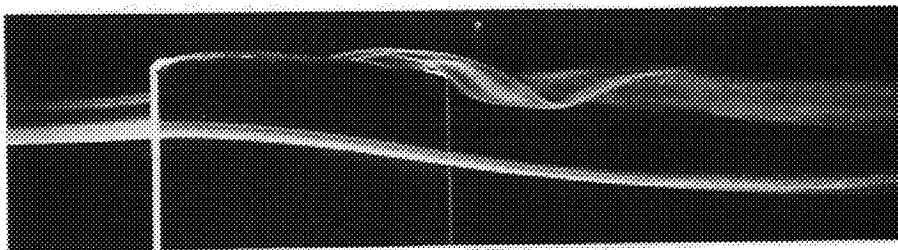
(h)

Figure 11. (Continued)
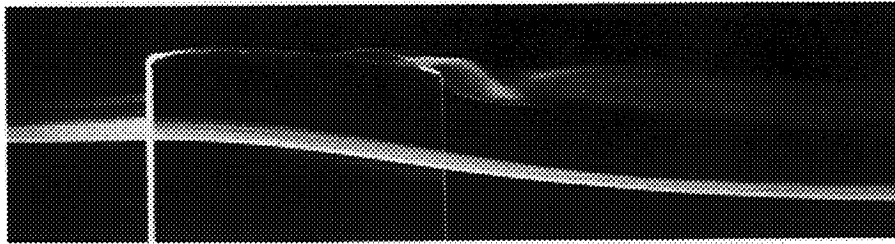
(i)

(j)
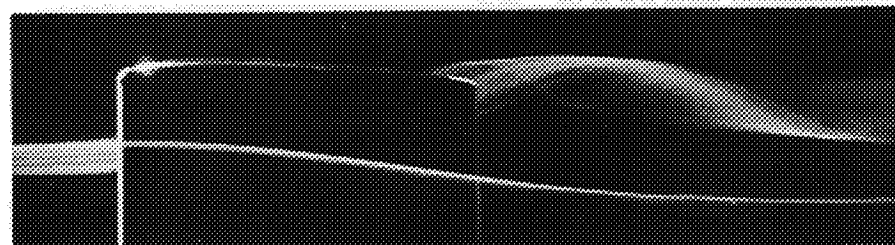
(k)
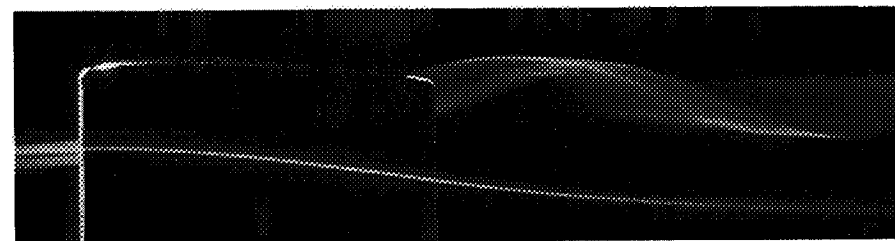
(l)

Figure 11. (Continued)

(a)

(b)

(c)

(d)
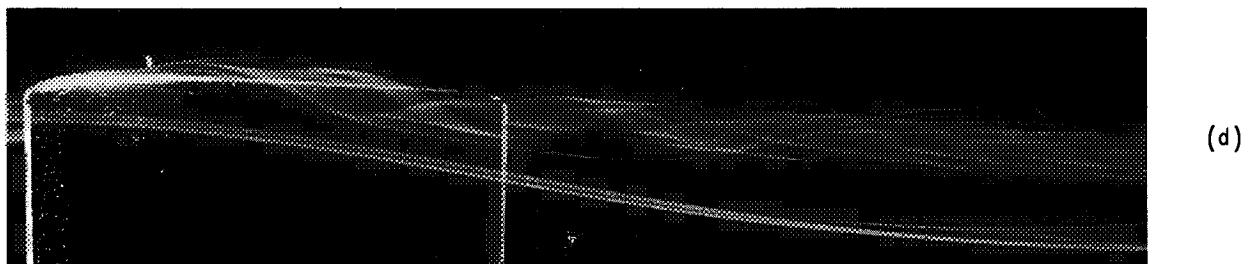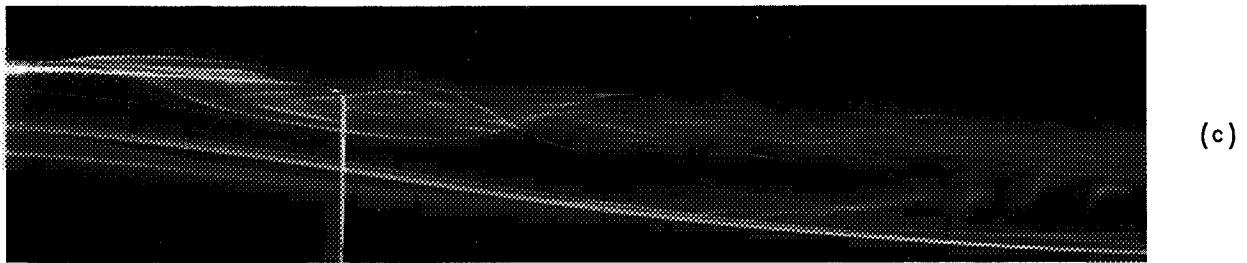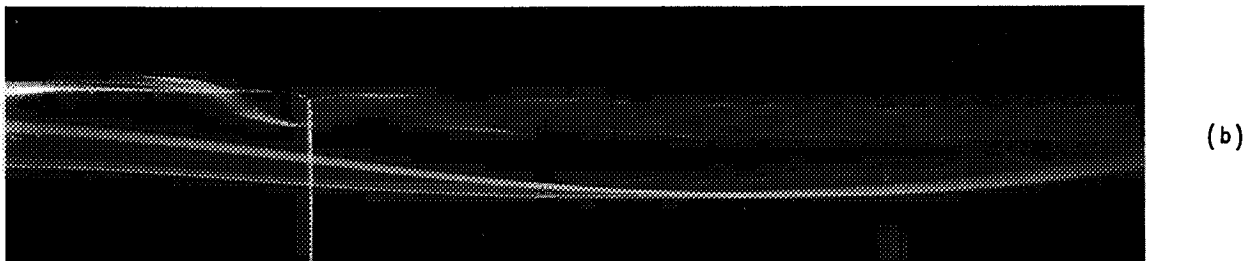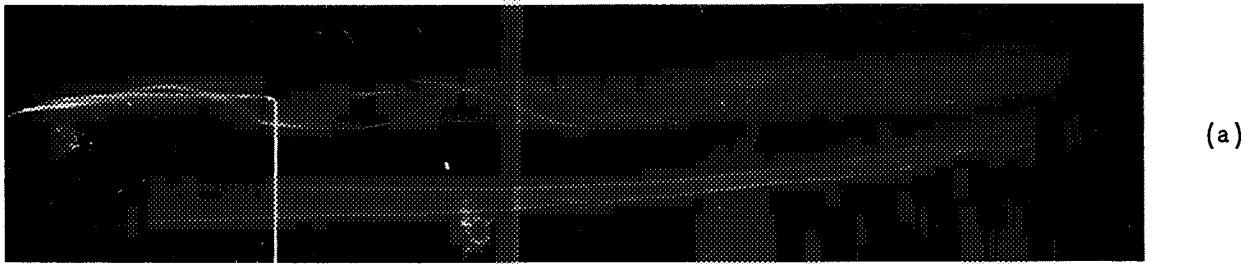
Figure 12. PHOTOGRAPHS SHOWING TIP VORTEX STRUCTURE; $V \approx 15$ fps; $\alpha = +9°$
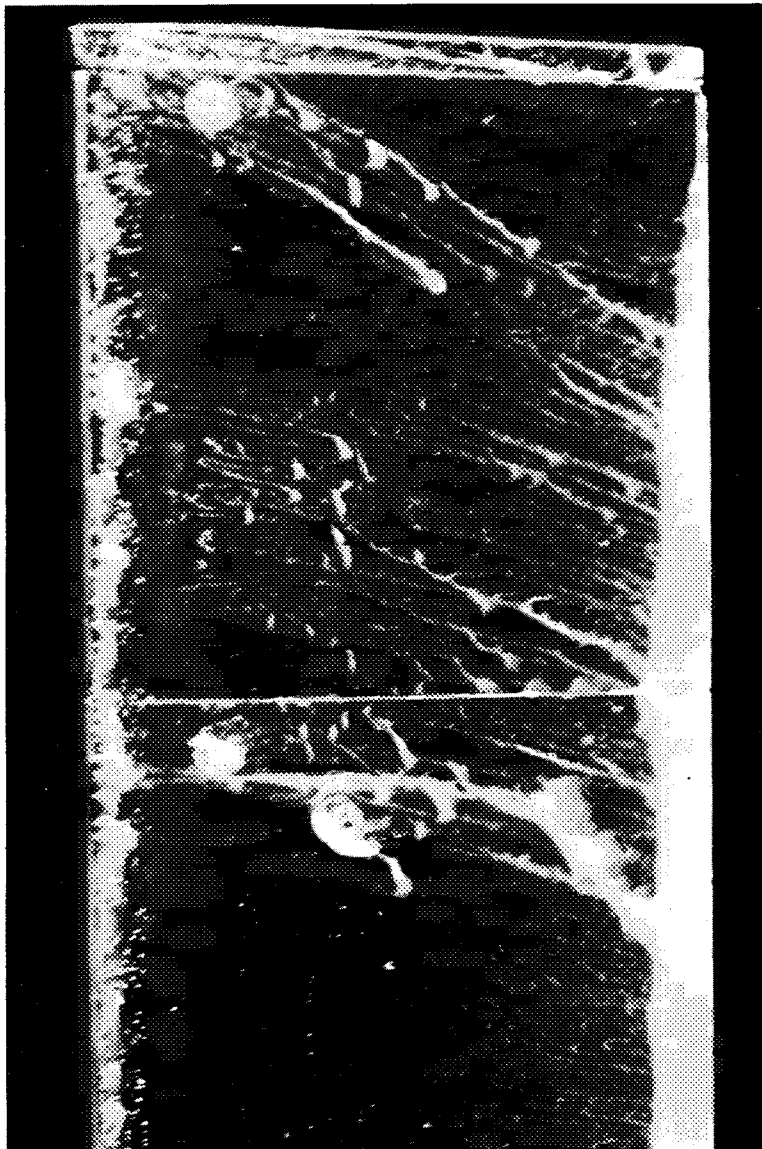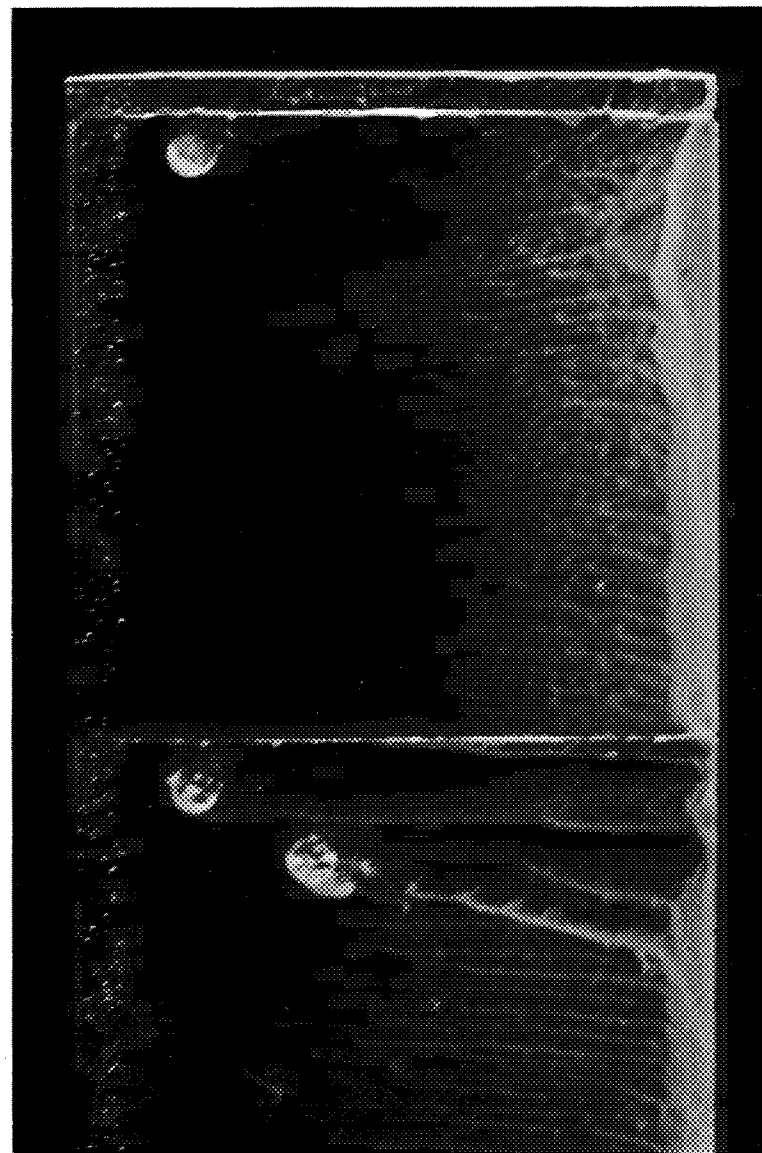
(a) $\alpha = +10°$ (b) $\alpha = -10°$

Figure 13. SURFACE OIL FLOW PATTERN ON BLUNT SQUARE TIP; $V \approx 115$ fps
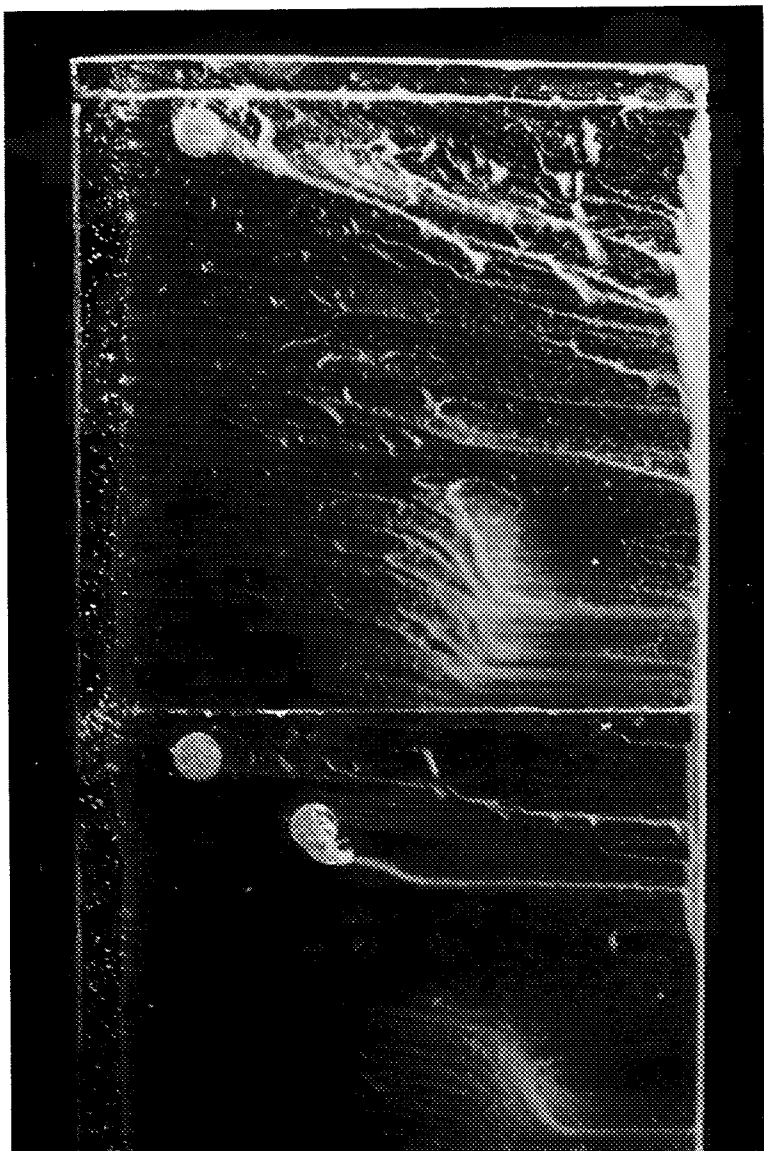
(c) $\alpha = 0°$

Figure 13. (Continued)

$\alpha = +10°$

(a)

$\alpha = +10°$

(b)

$\alpha = +10°$

(c)
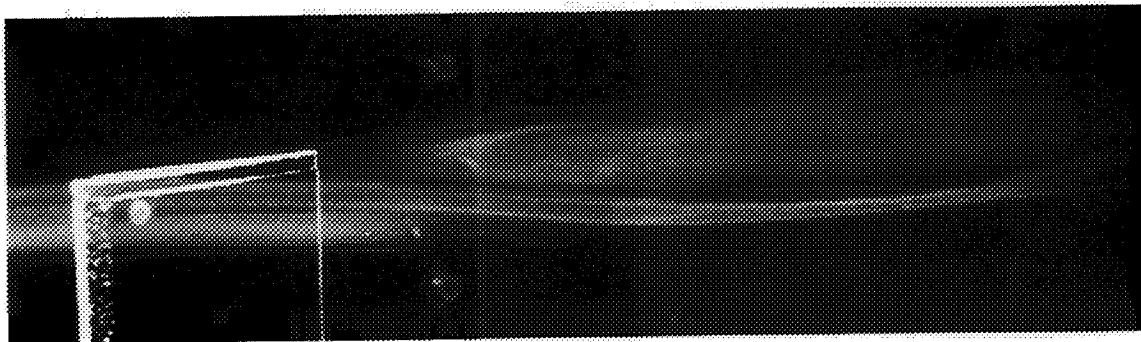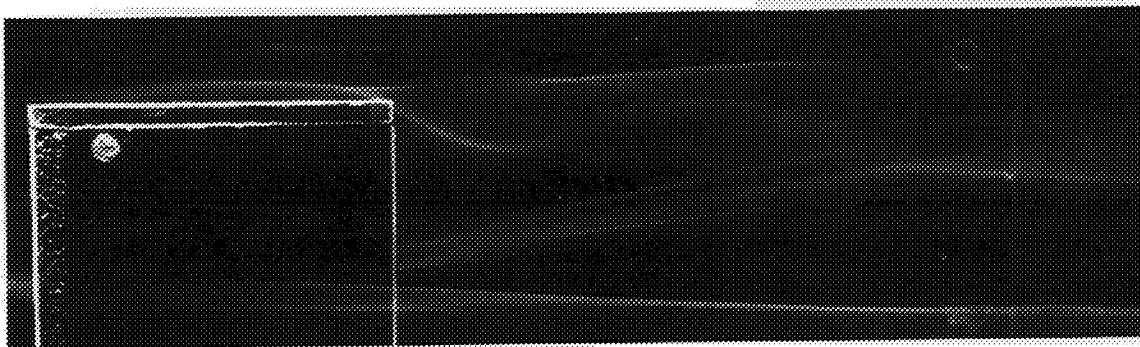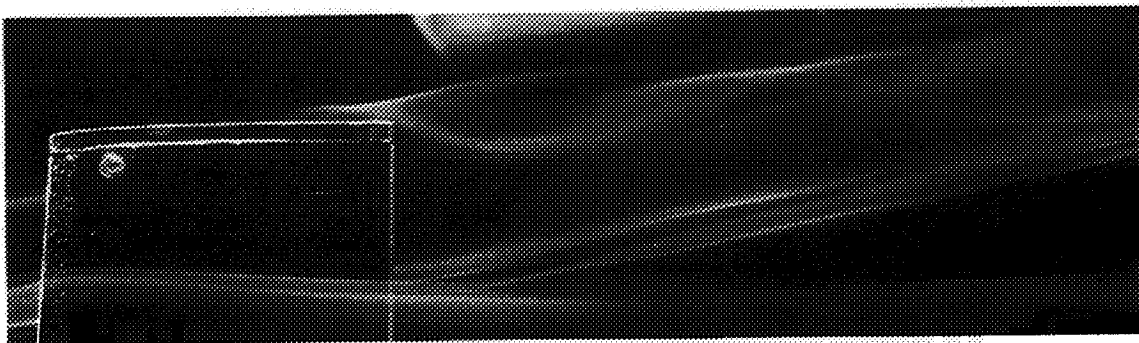
Figure 14. SMOKE FLOW ABOUT BLUNT SQUARE TIP; $V \approx 100$ fps
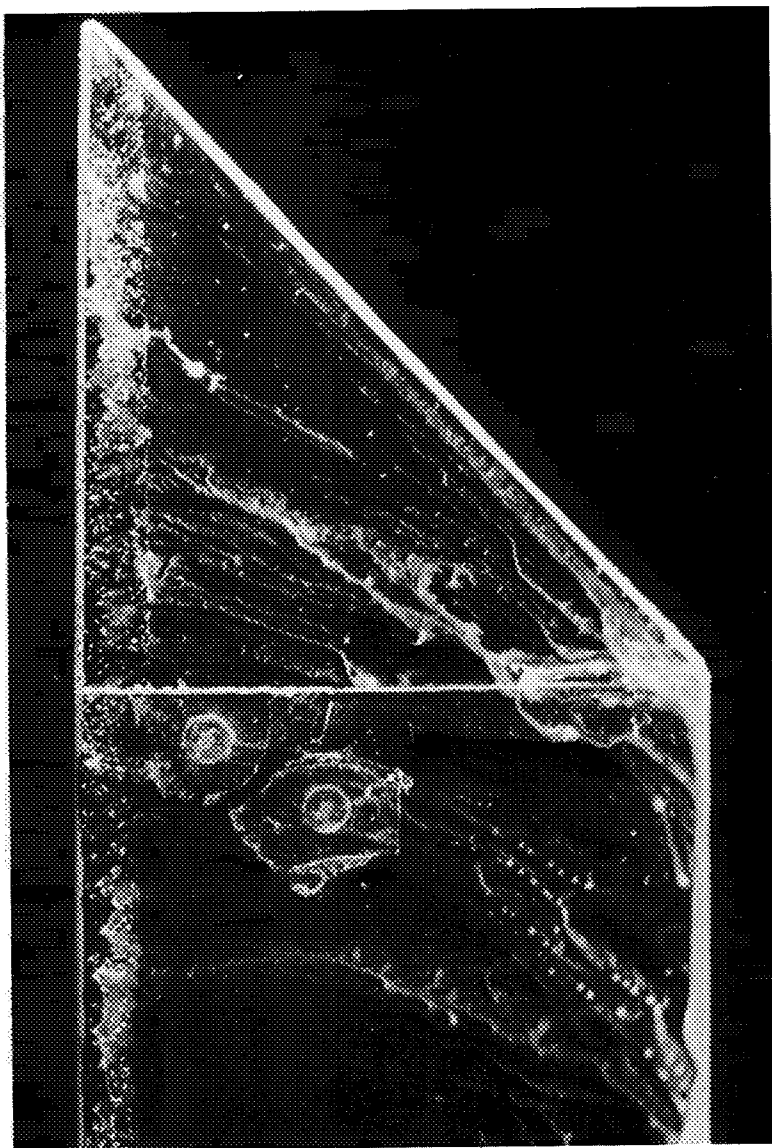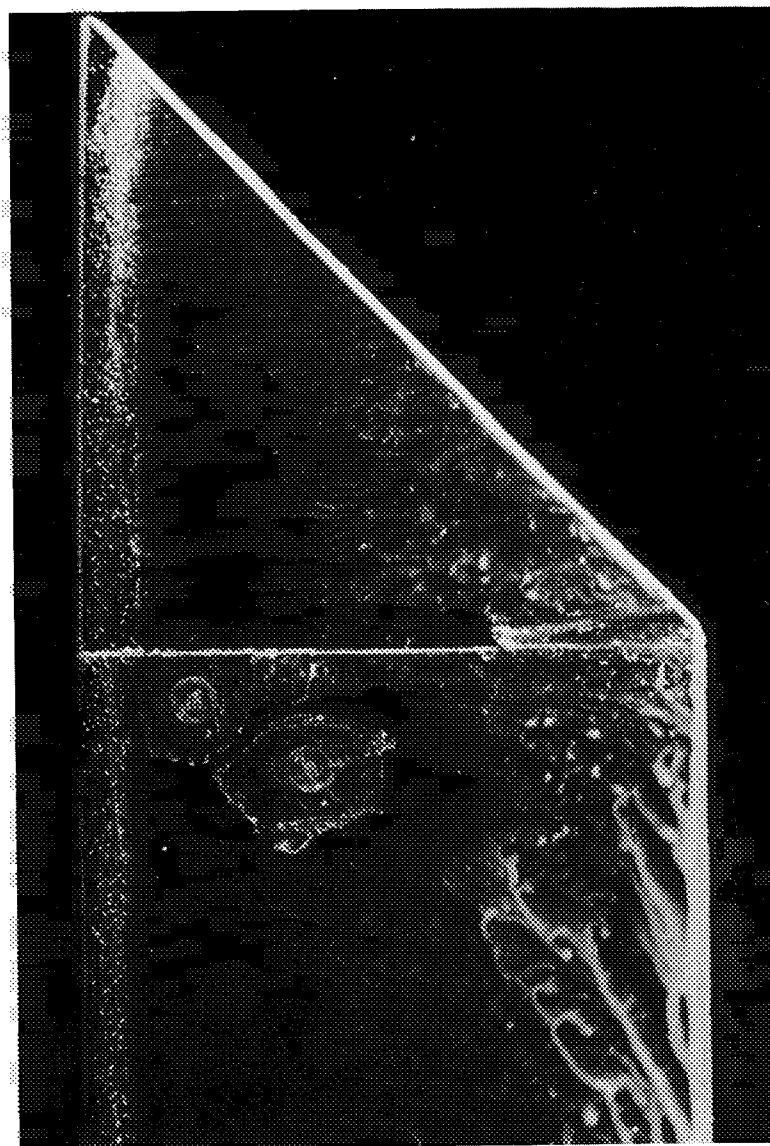
(a) $\alpha = +9°$ (b) $\alpha = -9°$

Figure 15. OIL SURFACE FLOW PATTERN ON SWEPT FORWARD 45° TIP; $V \approx 100$ fps

$\alpha = +10°$

$\alpha = +10°$
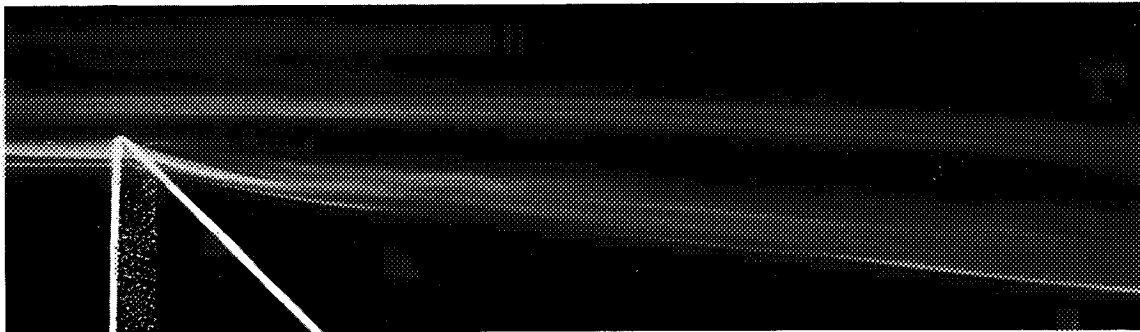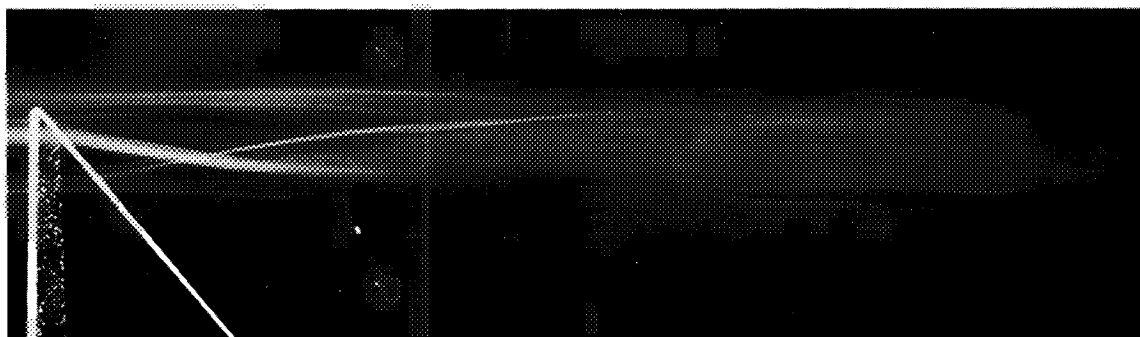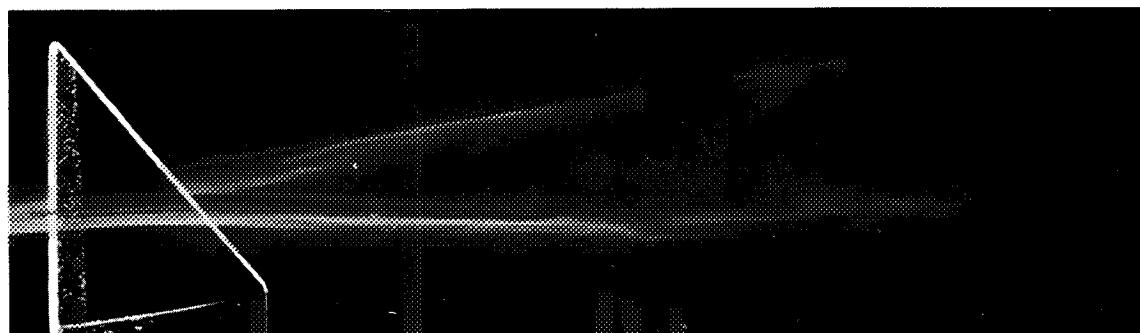
$\alpha = +10°$

Figure 16. SMOKE FLOW ABOUT SWEPT FORWARD 45° TIP; V≈100 fps
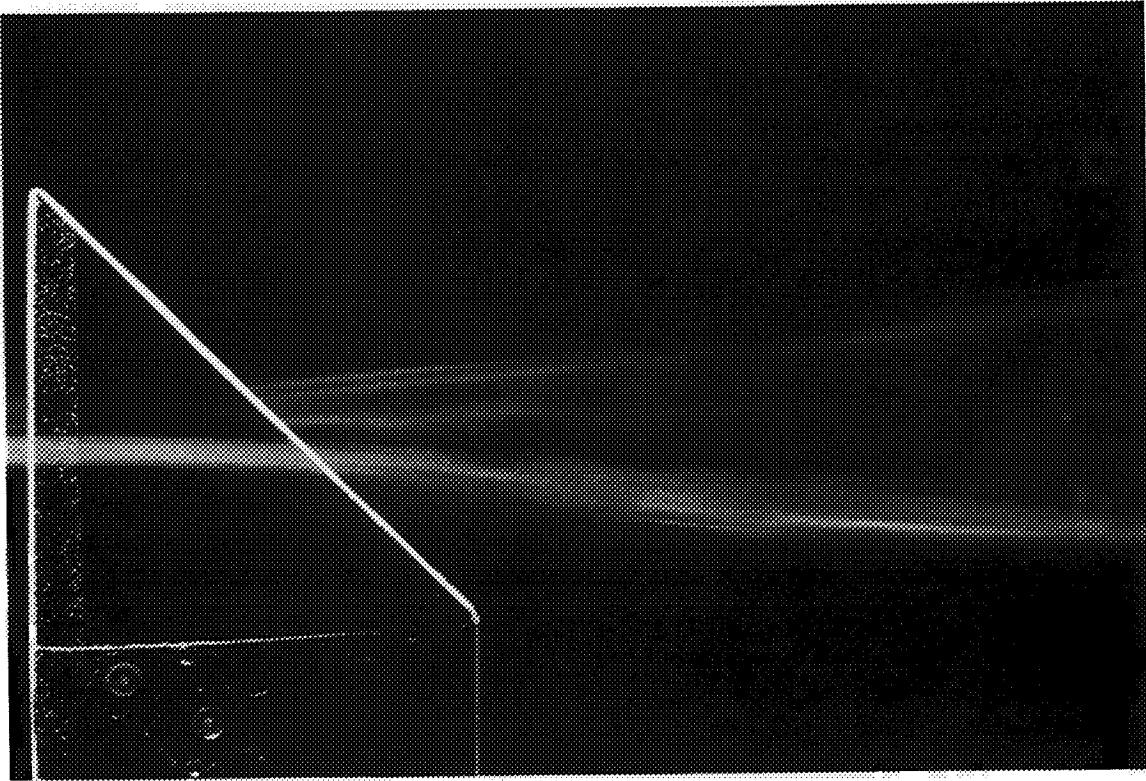
(d)

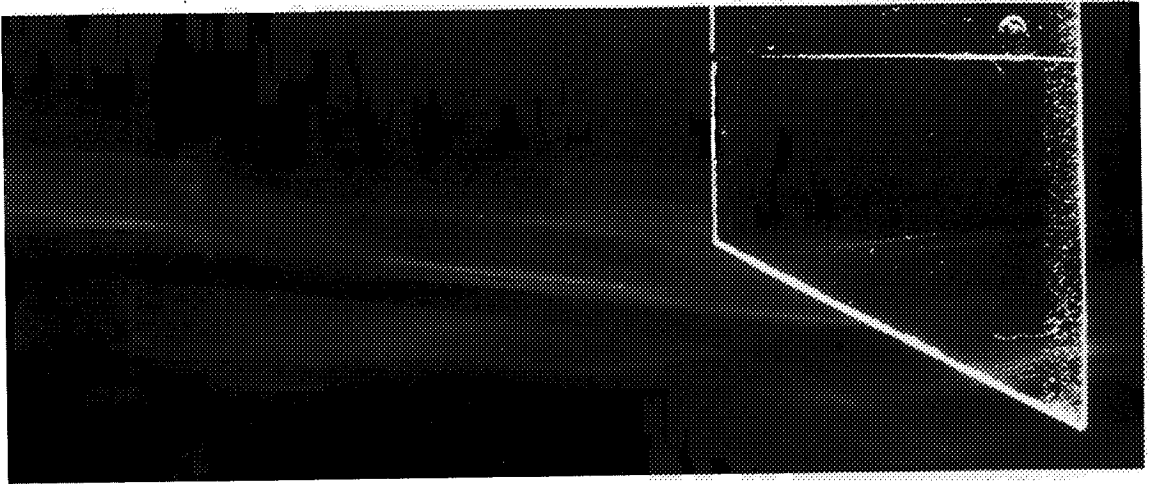$\alpha = +10°$

Figure 16. (Continued)

64
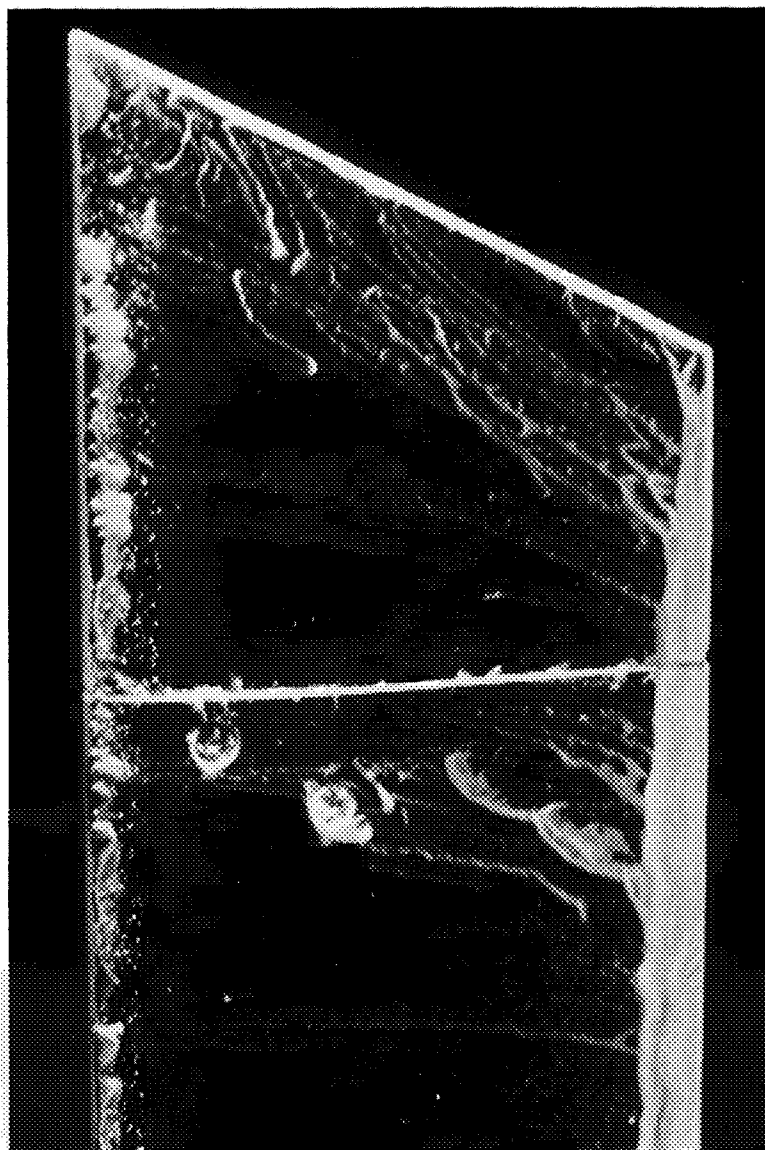
(a) $\alpha = +10°$
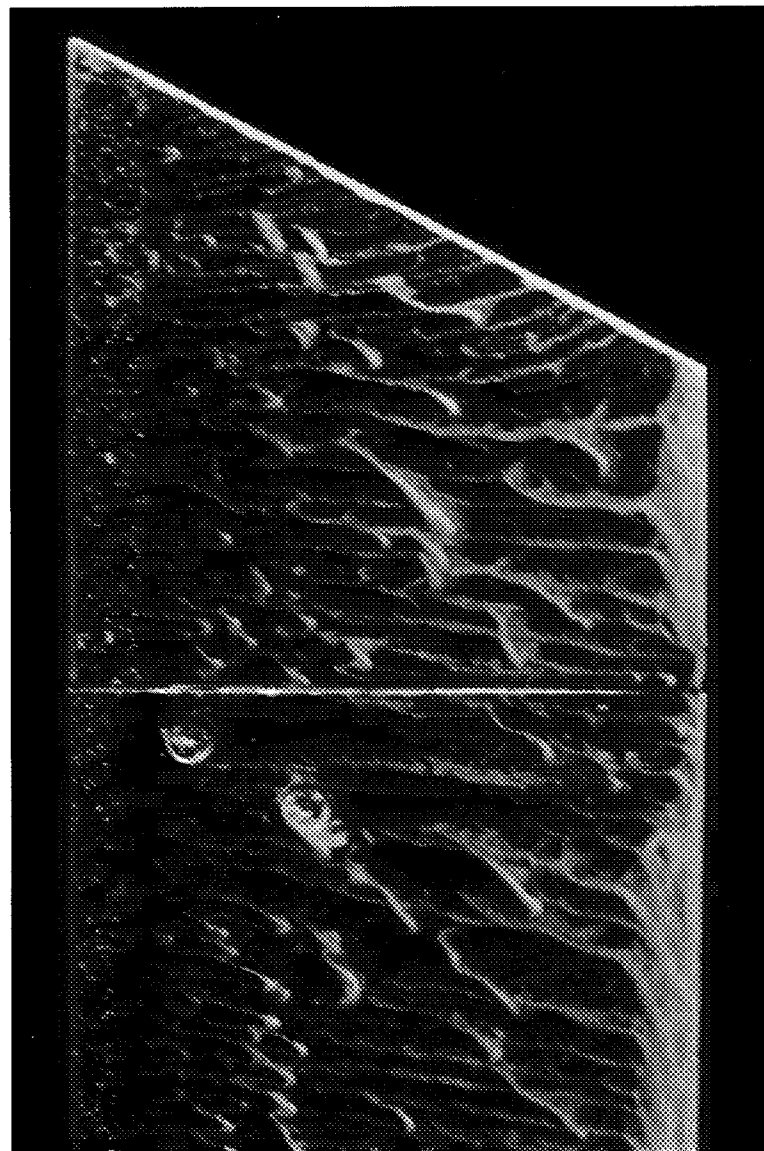
(b) $\alpha = -10°$

Figure 17. OIL SURFACE PATTERN ON SWEPT FORWARD 60° TIP; V≈115 fps

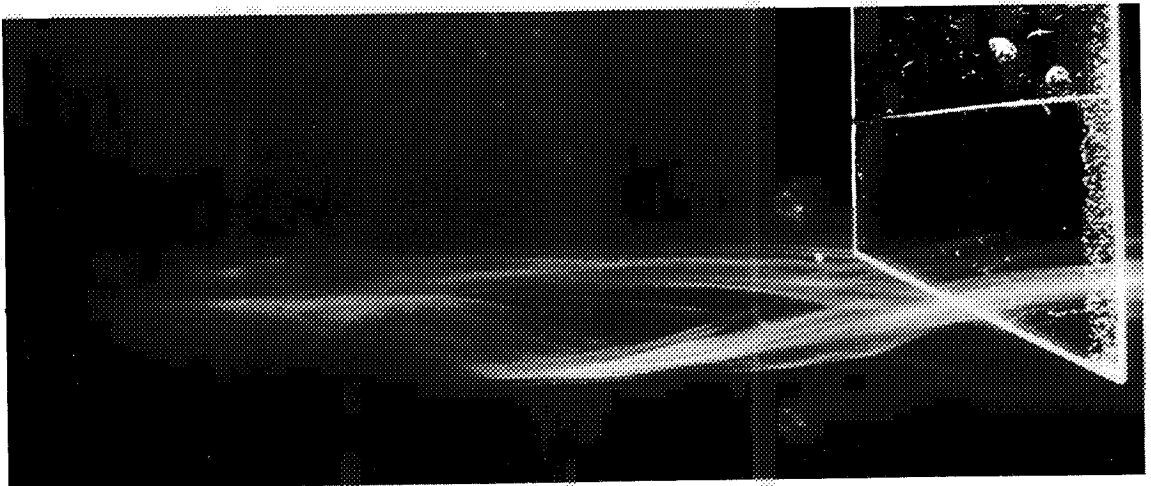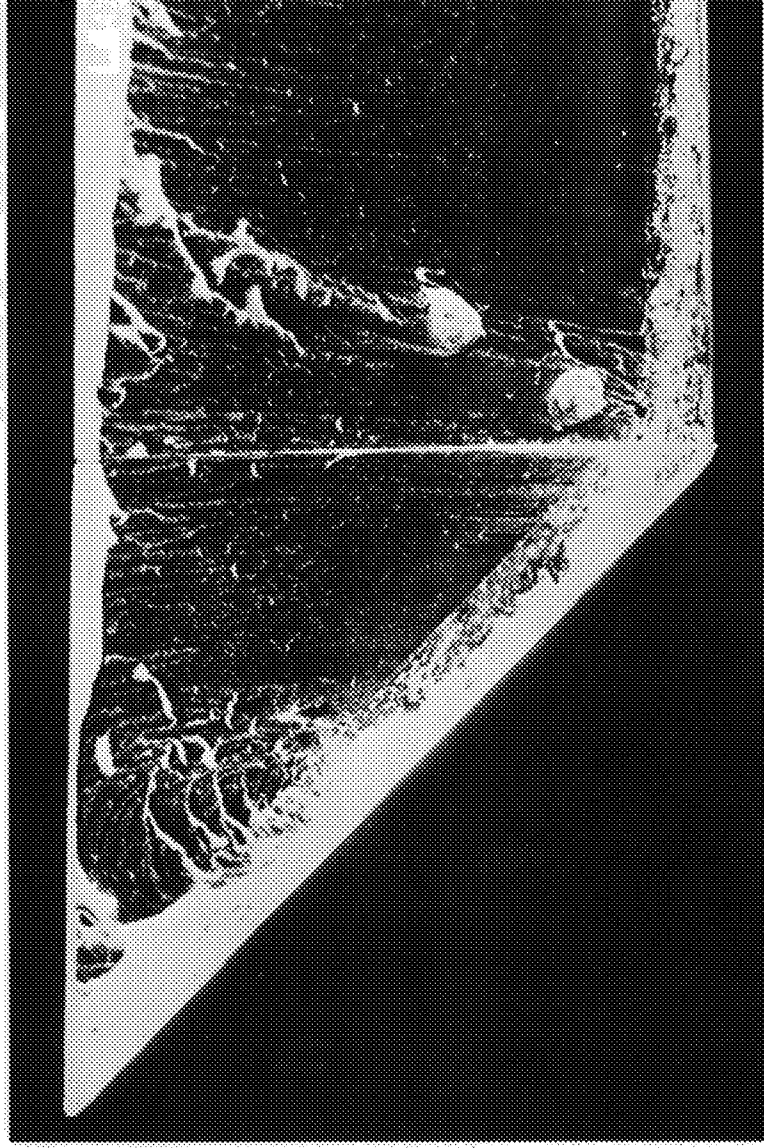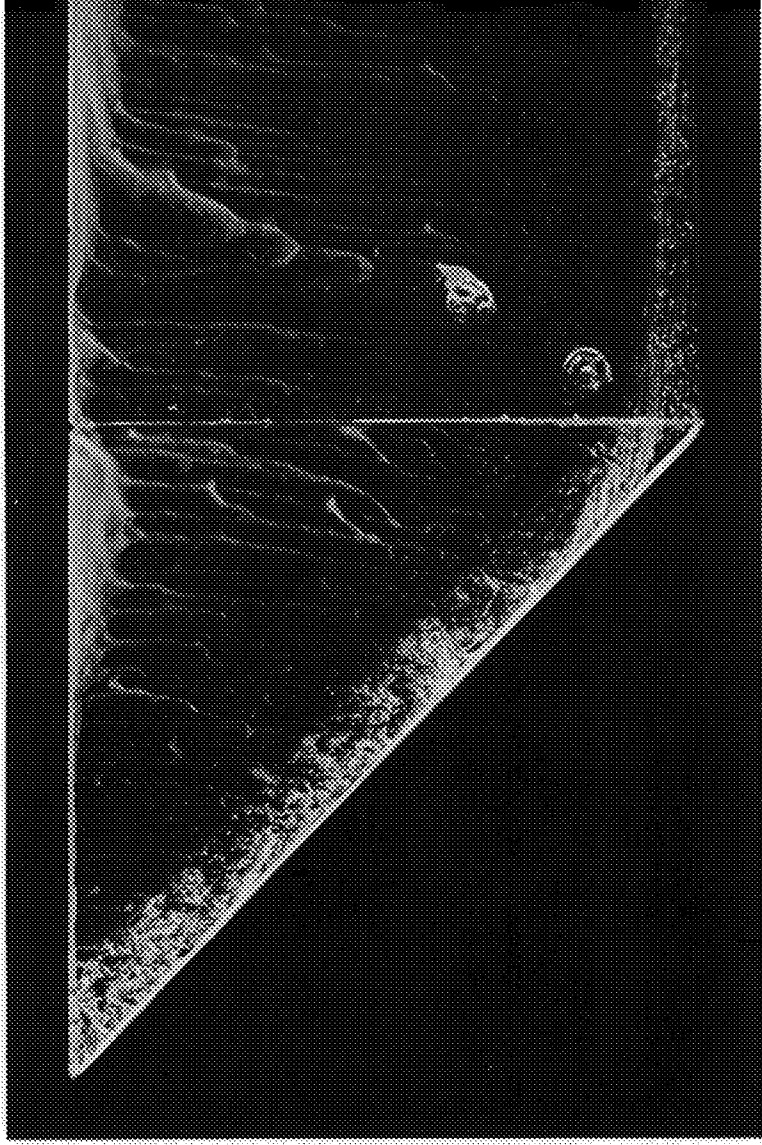Figure 19. OIL SURFACE FLOW PATTERN ON SWEPT AFT 45° TIP; V≈115 fps

(a) α = +10°

(b) α = -10°
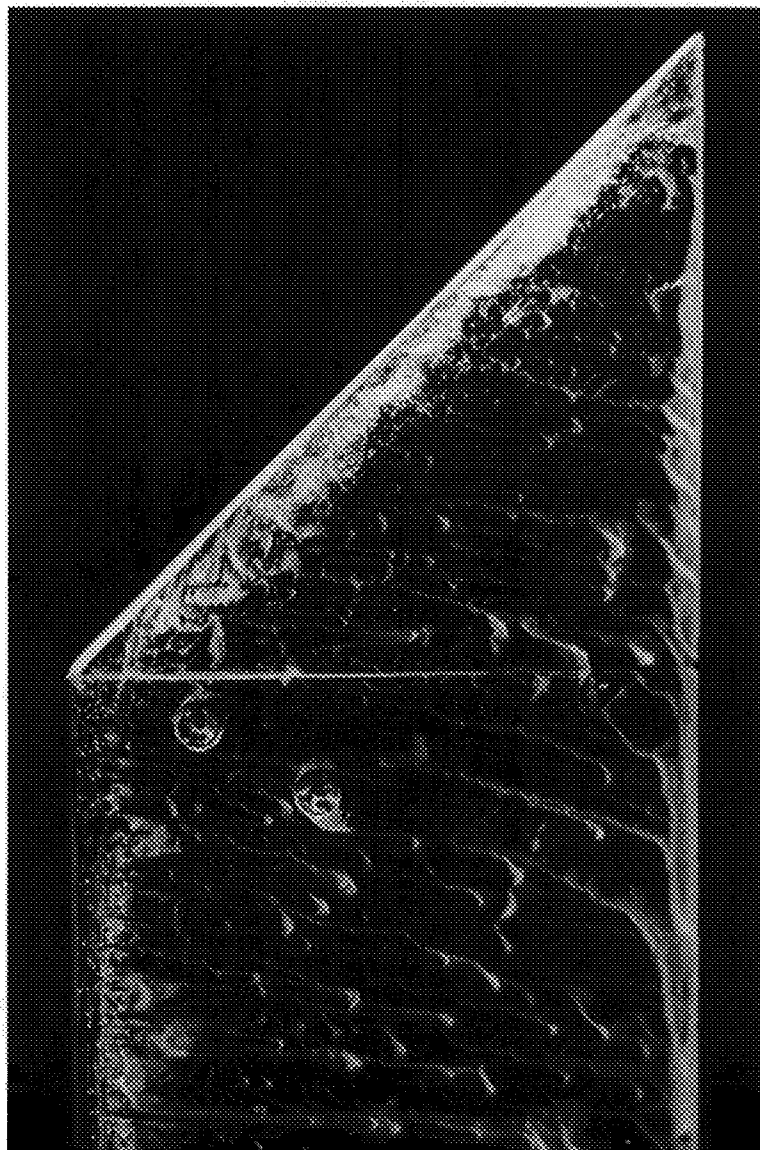
(c) $\alpha = +6°$

Figure 19. (Continued)

$\alpha = +10°$

$\alpha = +10°$
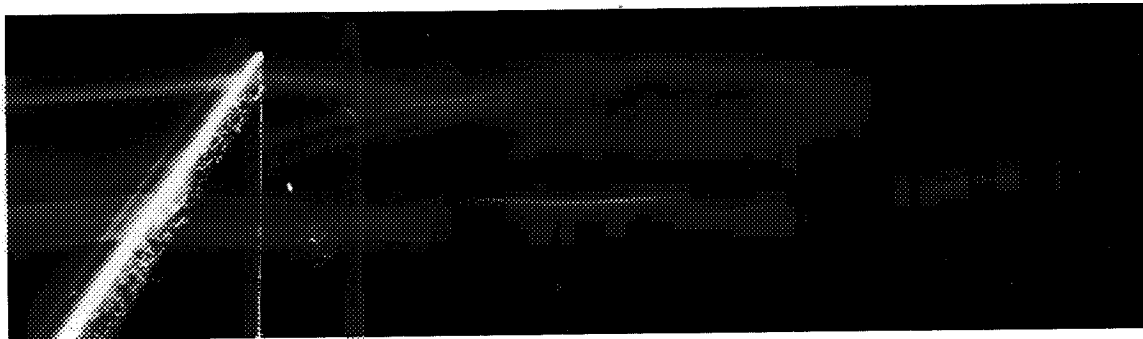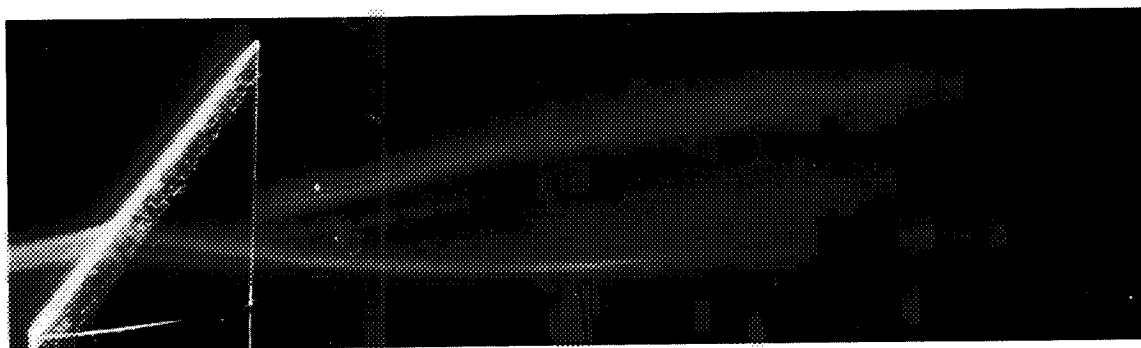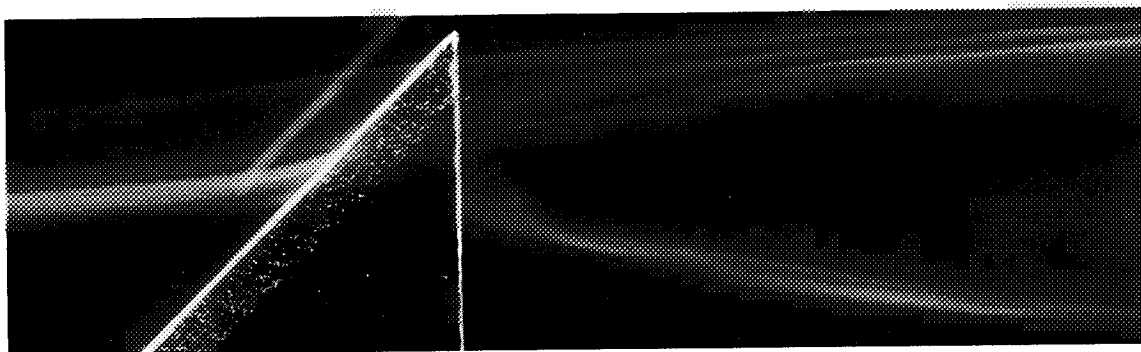
$\alpha = -10°$

Figure 20. SMOKE FLOW ABOUT SWEPT AFT 45° TIP; V≈115 fps
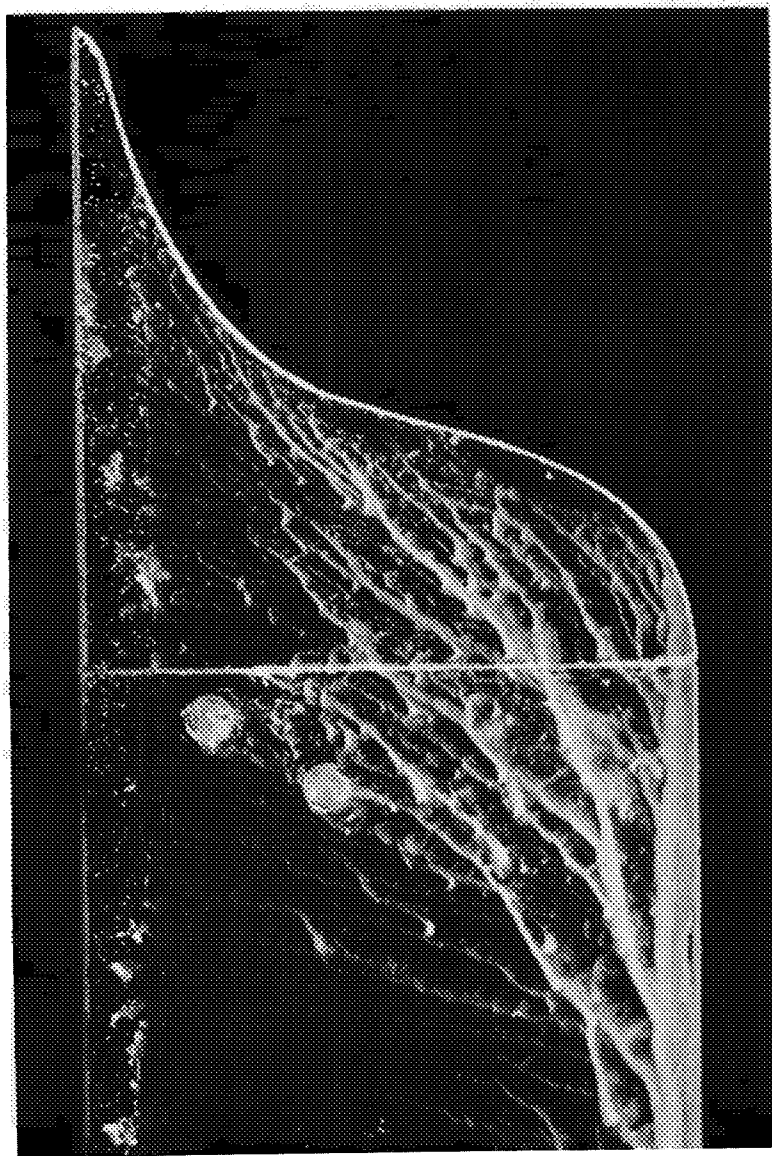
(a) $\alpha = +9°$
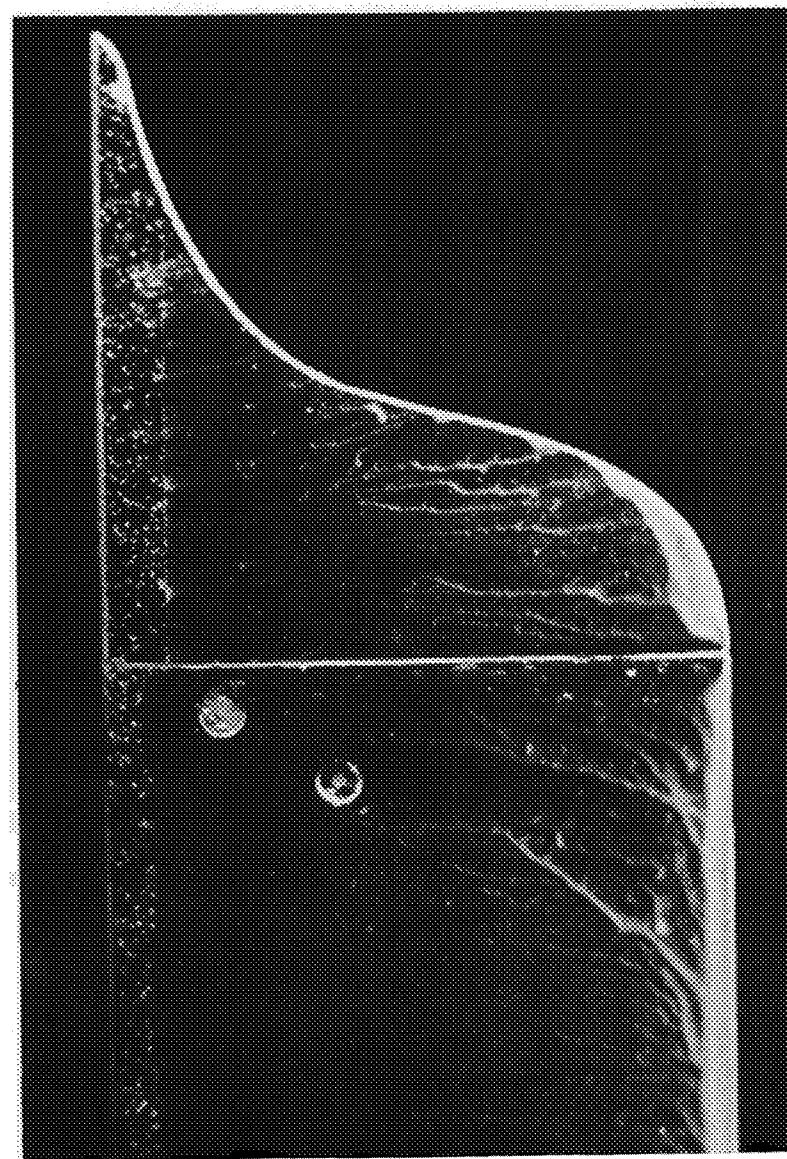
(b) $\alpha = -9°$

Figure 21. OIL SURFACE FLOW PATTERN ON CUSP TIP; $V \approx 100$ fps

$\alpha = +9°$

$\alpha = +9°$
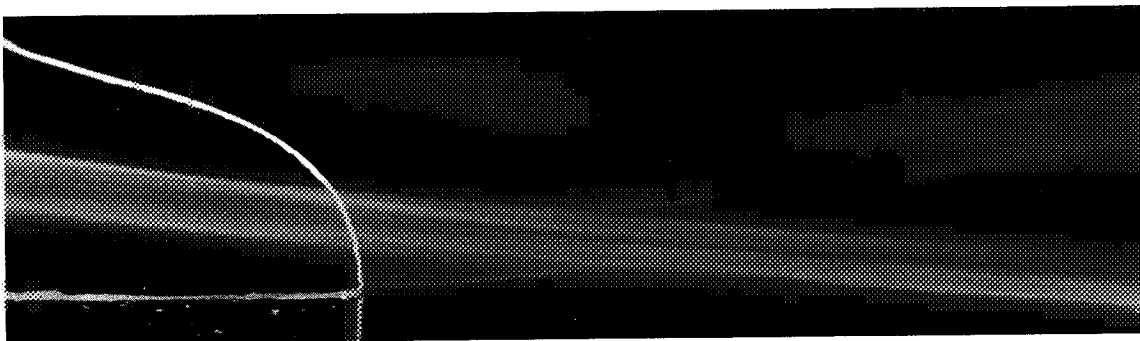
$\alpha = +9°$

Figure 22. SMOKE FLOW ABOUT CUSP TIP; V≈100 fps

Figure 23. PLOT OF EXPERIMENTAL WING LIFT
COEFFICIENT VS. WING DRAG
COEFFICIENT FOR ROUNDED SQUARE
TIP CONFIGURATION RUN 1

Figure 24. PLOT OF EXPERIMENTAL WING LIFT
COEFFICIENT VS. WING DRAG
COEFFICIENT FOR ROUNDED SQUARE
TIP CONFIGURATION RUN 2

WING LIFT COEFFICIENT

WING DRAG COEFFICIENT

○ - ANGLE OF ATTACK INCREASED IN MAGNITUDE
□ - ANGLE OF ATTACK DECREASED IN MAGNITUDE

WING AREA: 47.9 sq in.
TUNNEL DYNAMIC PRESSURE: 0.0993 psi
WALL SUCTION: 50 mm

Figure 25. PLOT OF EXPERIMENTAL WING LIFT
COEFFICIENT VS. WING DRAG
COEFFICIENT FOR ROUNDED SQUARE
TIP CONFIGURATION RUN 3

WING LIFT COEFFICIENT

WING DRAG COEFFICIENT

○ - ANGLE OF ATTACK INCREASED IN MAGNITUDE
□ - ANGLE OF ATTACK DECREASED IN MAGNITUDE

WING AREA: 47.9 sq in.
TUNNEL DYNAMIC PRESSURE: 0.1100 psi
WALL SUCTION: 50 mm

Figure 26. PLOT OF EXPERIMENTAL WING LIFT
COEFFICIENT VS. WING DRAG
COEFFICIENT FOR ROUNDED SQUARE
TIP CONFIGURATION RERUN AT A
HIGHER DYNAMIC PRESSURE

73

74

Figure 27 (left plot):

WING LIFT COEFFICIENT

0.8

0.4

0

-0.4

-0.8

○ – ANGLE OF ATTACK INCREASED IN MAGNITUDE
□ – ANGLE OF ATTACK DECREASED IN MAGNITUDE

WING AREA: 42.0 sq in.
TUNNEL DYNAMIC PRESSURE: 0.0994 psi
WALL SUCTION: 50 mm

-0.01   0   0.02   0.04

WING DRAG COEFFICIENT

Figure 27. PLOT OF EXPERIMENTAL WING LIFT
COEFFICIENT VS. WING DRAG
COEFFICIENT FOR SWEPT FORWARD
45° TIP CONFIGURATION

Figure 28 (right plot):

WING LIFT COEFFICIENT

0.8

0.4

0

-0.4

-0.8

○ – ANGLE OF ATTACK INCREASED IN MAGNITUDE
□ – ANGLE OF ATTACK DECREASED IN MAGNITUDE

WING AREA: 42.0 sq in.
TUNNEL DYNAMIC PRESSURE: 0.1000 psi
WALL SUCTION: 30 mm

-0.01   0   0.02   0.04

WING DRAG COEFFICIENT

Figure 28. PLOT OF EXPERIMENTAL WING LIFT
COEFFICIENT VS. WING DRAG
COEFFICIENT FOR SWEPT FORWARD
45° TIP CONFIGURATION
RERUN AT LOWER VACUUM
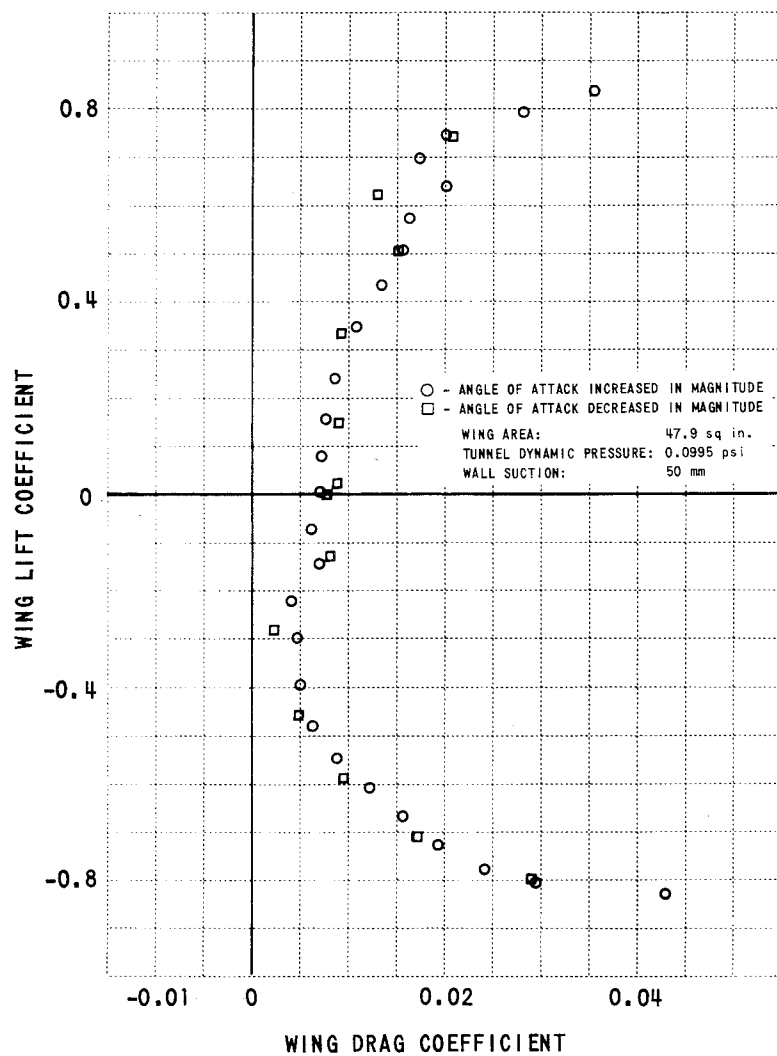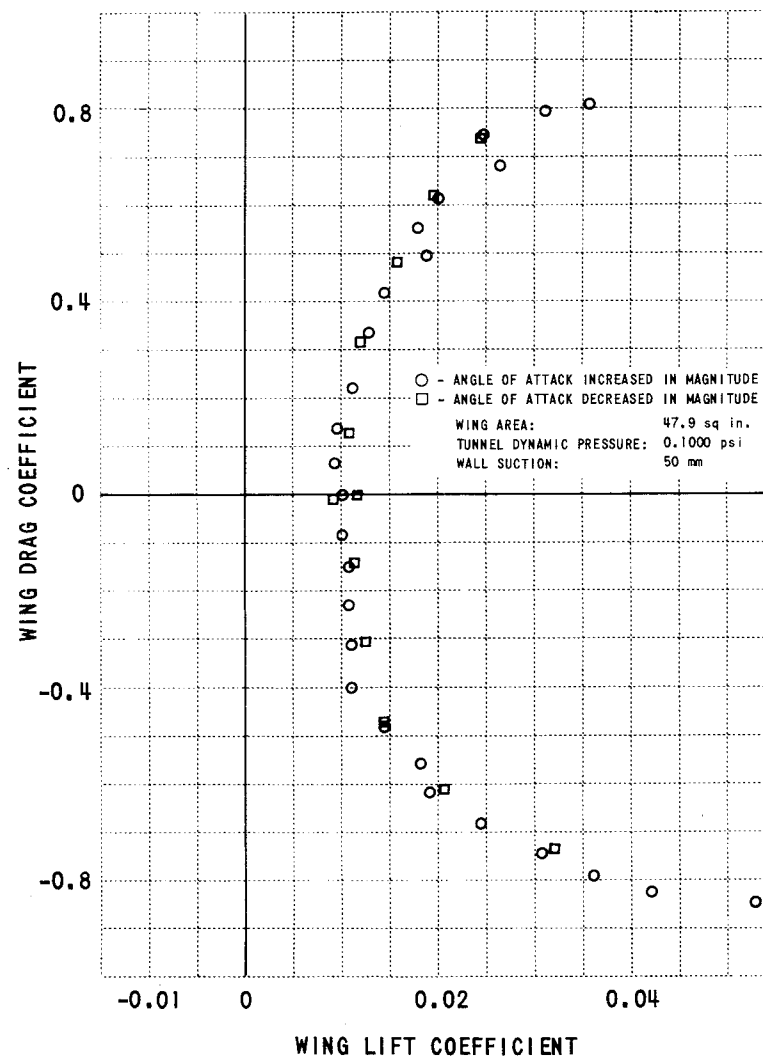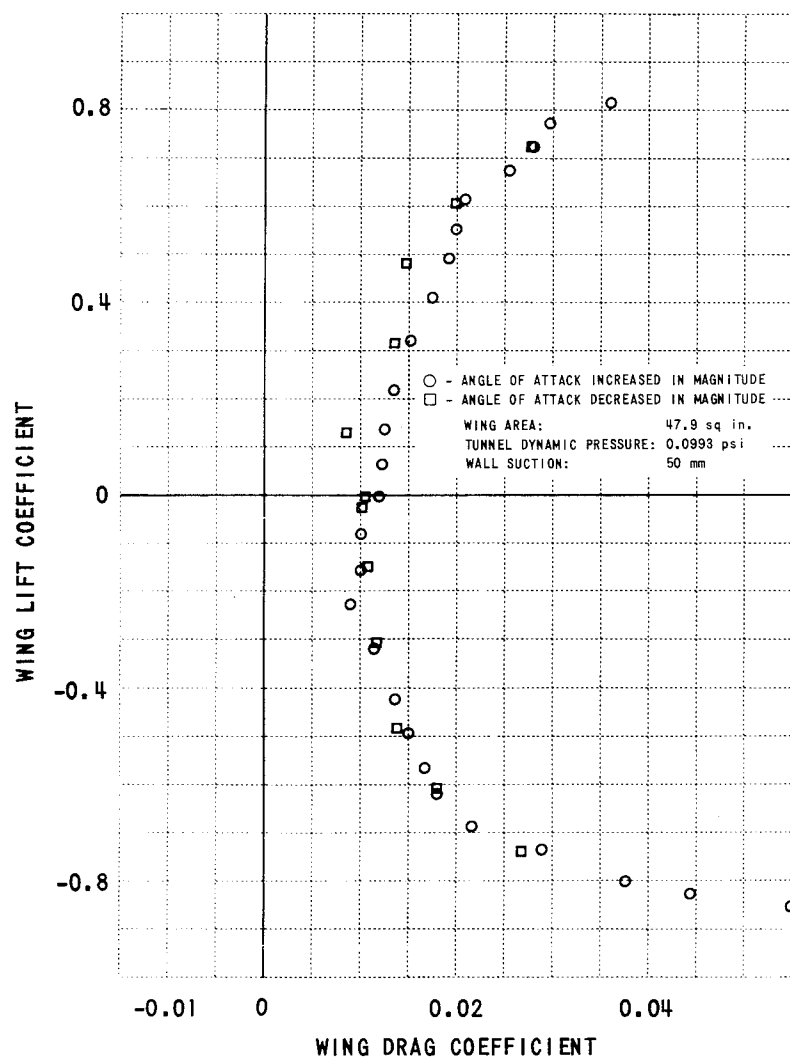
Figure 29. PLOT OF EXPERIMENTAL WING LIFT COEFFICIENT VS. WING DRAG COEFFICIENT FOR BLUNTED SQUARE TIP CONFIGURATION
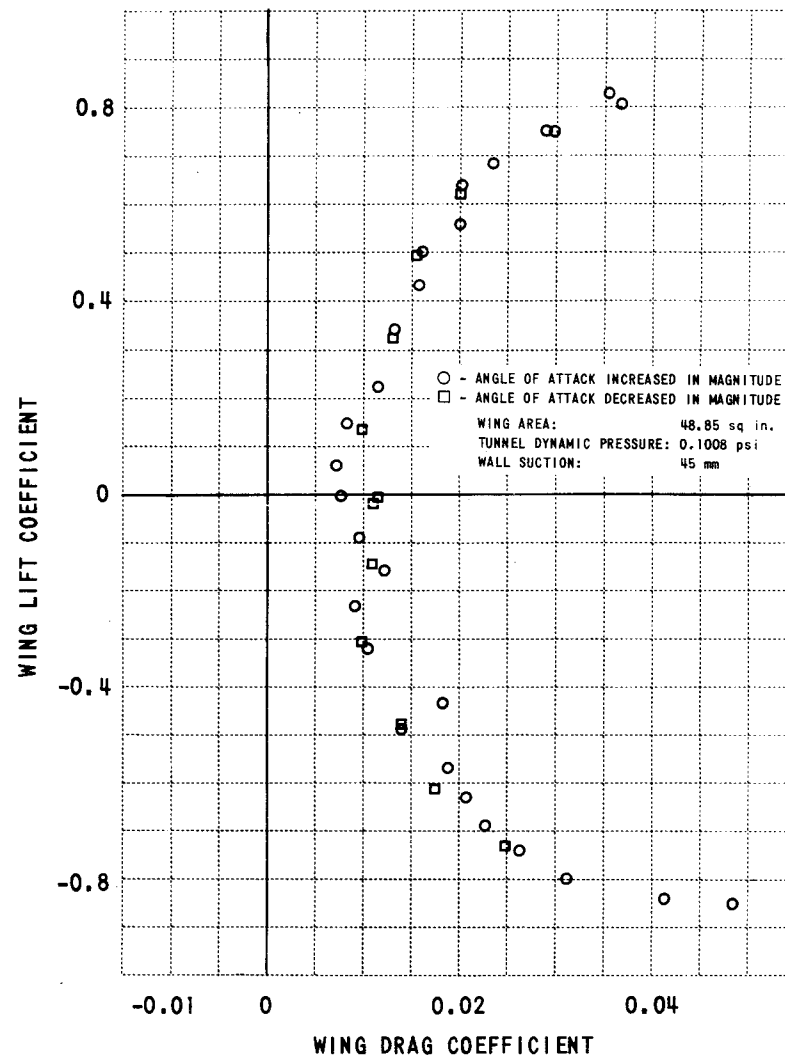
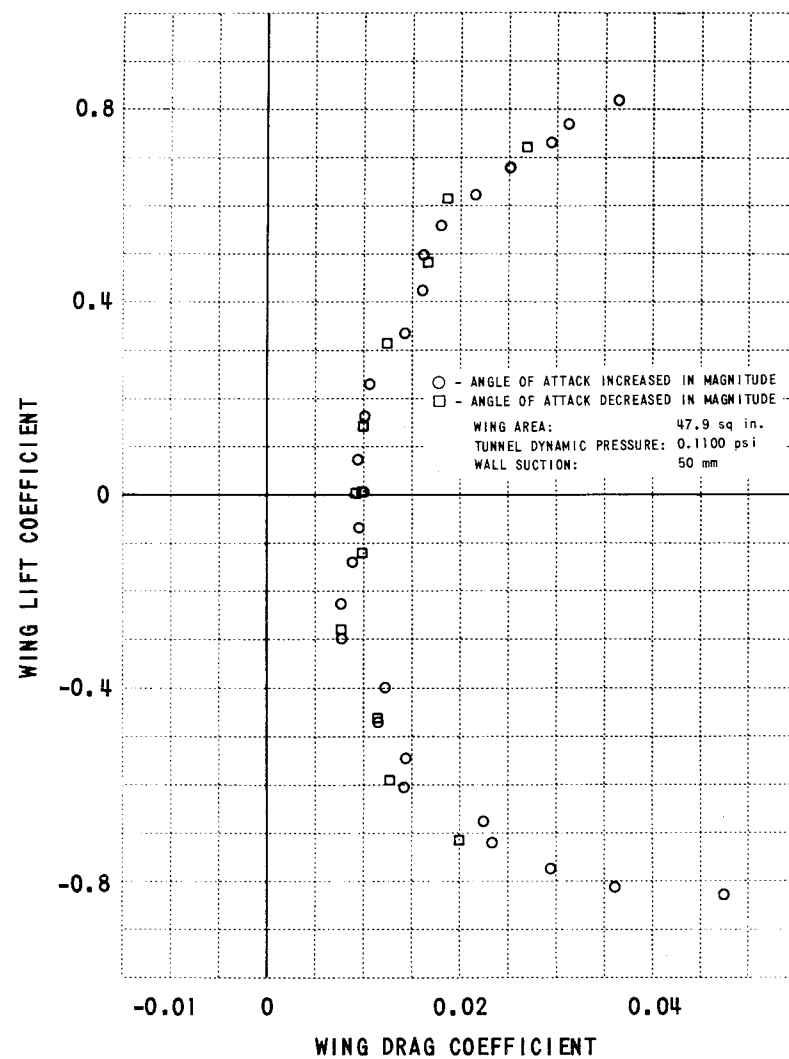Figure 30. PLOT OF EXPERIMENTAL WING LIFT COEFFICIENT VS. WING DRAG COEFFICIENT FOR BLUNTED SQUARE TIP CONFIGURATION WITH A SLIGHTLY LONGER SPAN
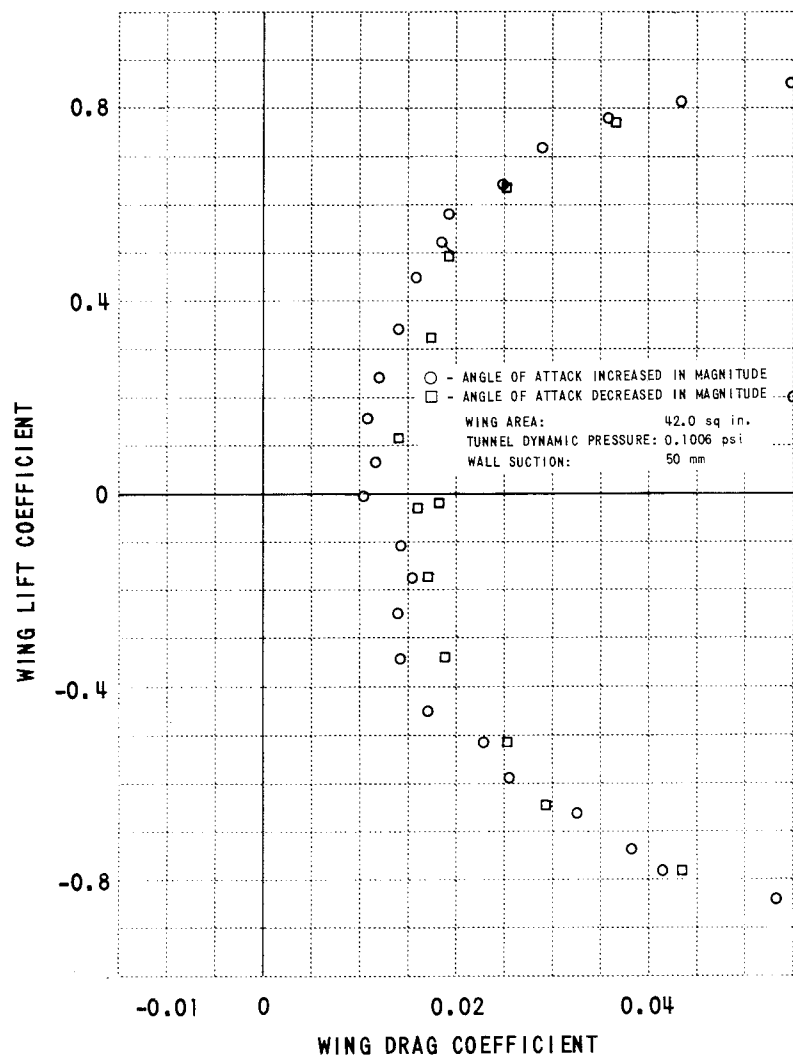
Figure 31. PLOT OF EXPERIMENTAL WING LIFT
COEFFICIENT VS. WING DRAG
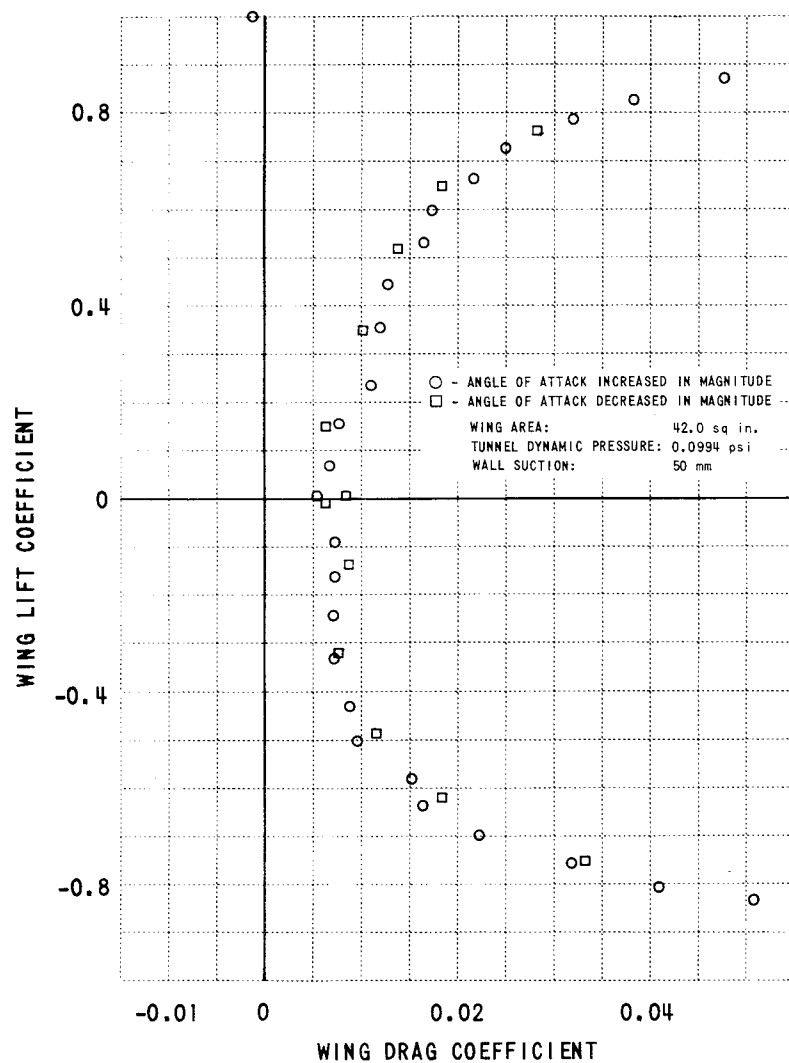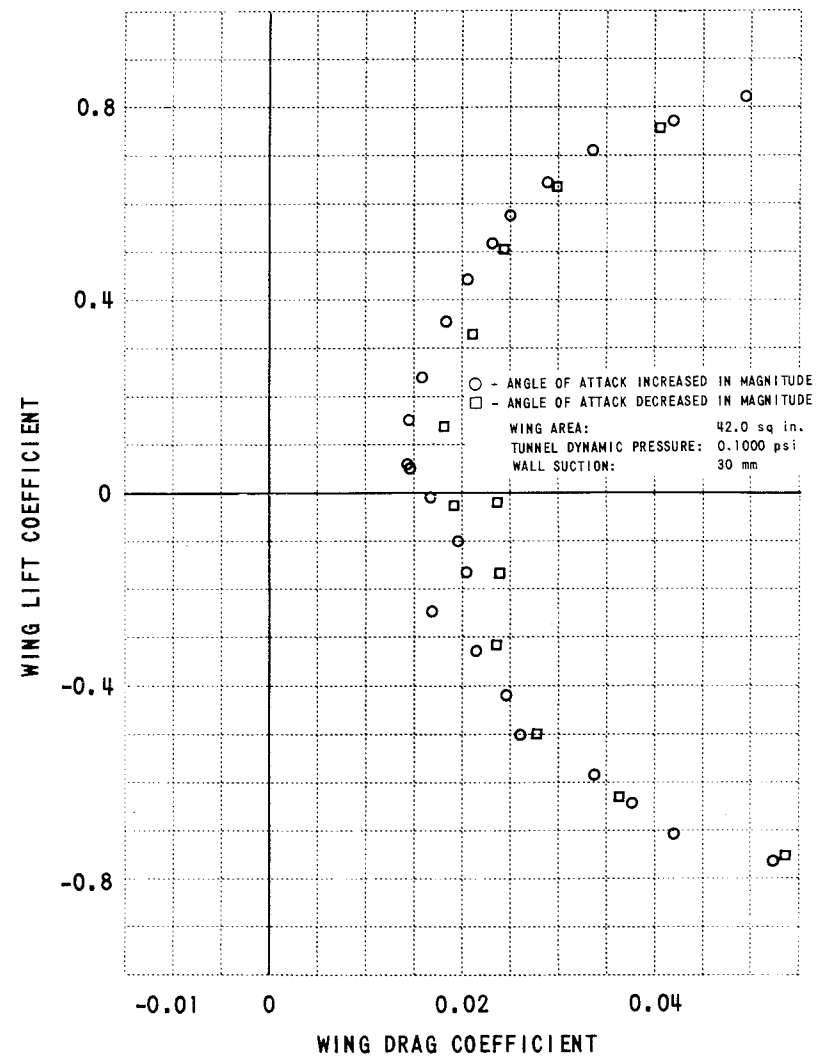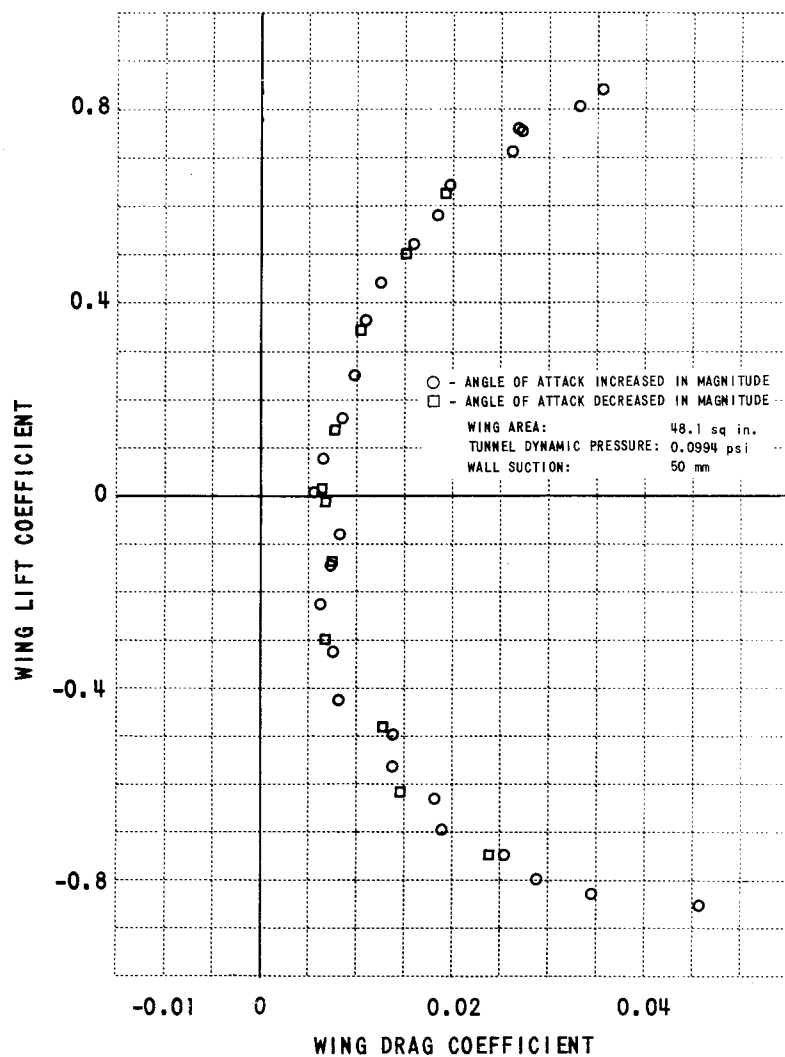COEFFICIENT FOR SWEPT AFT 45°
TIP CONFIGURATION

Figure 32. PLOT OF EXPERIMENTAL WING LIFT
COEFFICIENT VS. WING DRAG
COEFFICIENT FOR SWEPT FORWARD
60° TIP CONFIGURATION

Figure 33. PLOT OF EXPERIMENTAL WING LIFT
COEFFICIENT VS. WING DRAG
COEFFICIENT FOR CUSPED
TIP CONFIGURATION

No.
Copies

NASA Langley Research Center
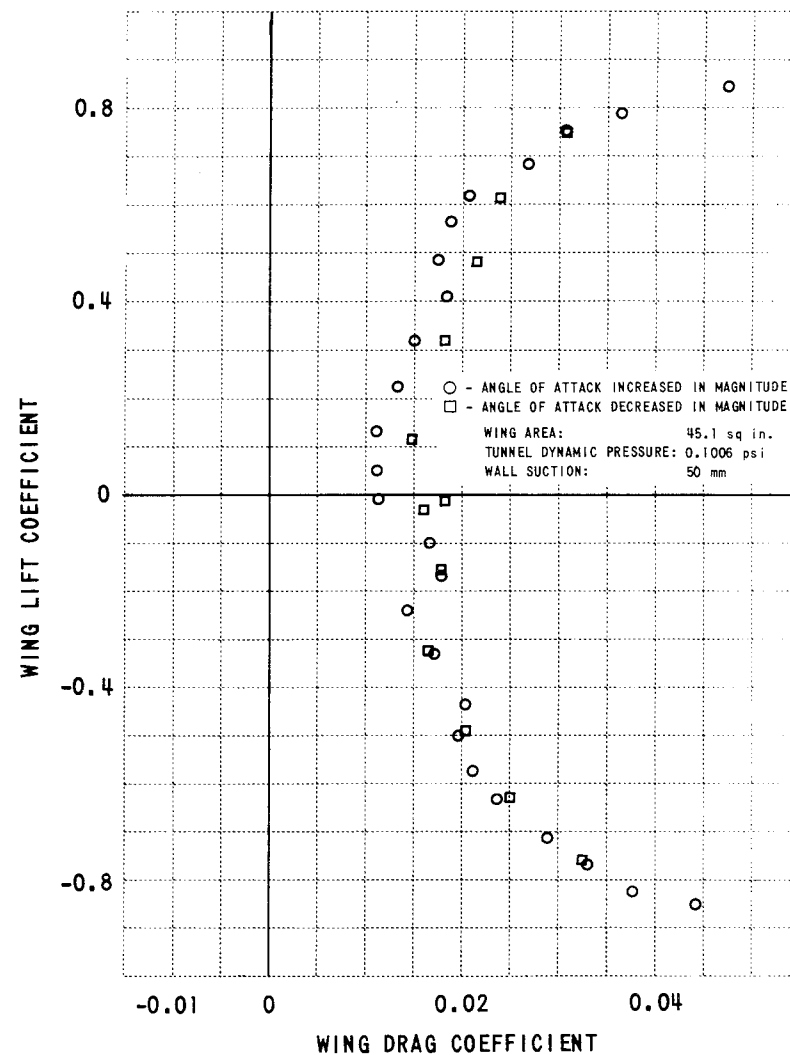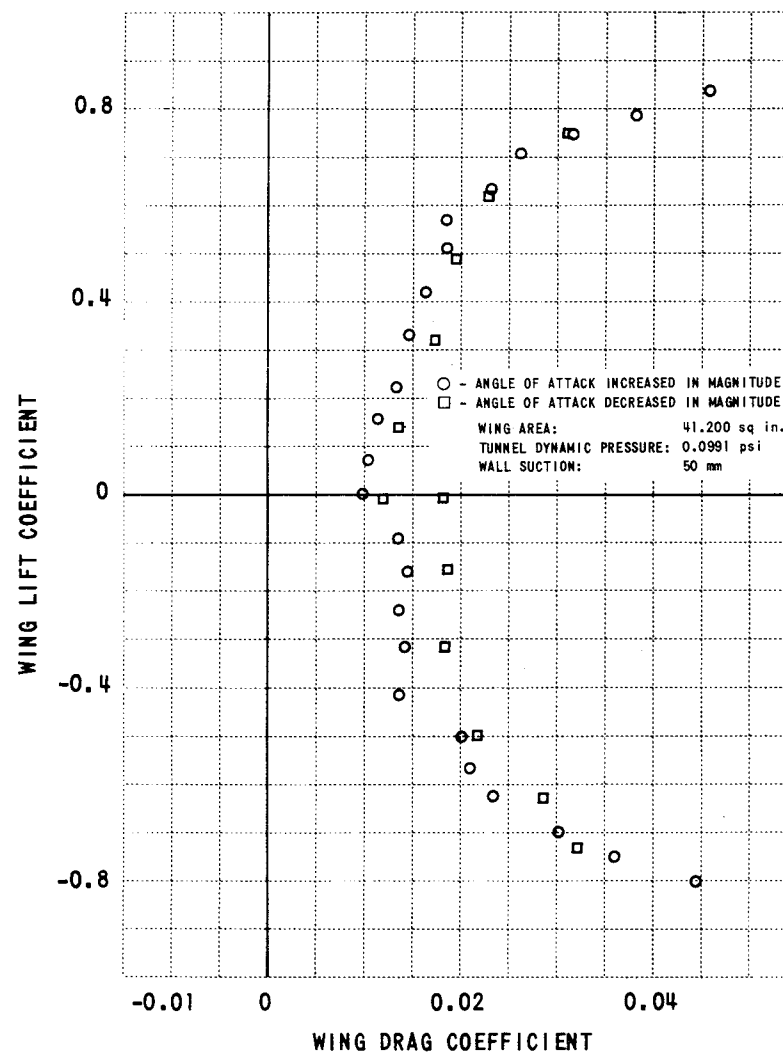Langley Station
Hampton, Virginia   23365
Attention: Research Program Records Unit, Mail Stop 122   1
             Raymond L. Zavasky, Mail Stop 117   1
             John F. Ward, Mail Stop 249   10

NASA Ames Research Center
Moffett Field, California   94035
Attention: Library, Stop 202-3   1

NASA Flight Research Center
P. O. Box 273
Edwards, California   93523
Attention: Library   1

Jet Propulsion Laboratory
4800 Oak Grove Drive
Pasadena, California   91103
Attention: Library, Mail 111-113   1

NASA Manned Spacecraft Center
2101 Webster Seabrook Road
Houston, Texas   77058
Attention: Library, Code BM6   1

NASA Marshall Space Flight Center
Huntsville, Alabama   35812
Attention: Library   1

NASA Wallops Station
Wallops Island, Virginia   23337
Attention: Library   1

NASA Electronics Research Center
575 Technology Square
Cambridge, Massachusetts   02139
Attention: Library   1

NASA Lewis Research Center
21000 Brookpark Road
Cleveland, Ohio   44135
Attention: Library, Mail STop 60-3   1

NASA Goddard Space Flight Center
Greenbelt, Maryland   20771
Attention: Library   1

NASA John F. Kennedy Space Center
Kennedy Space Center, Florida   32899
Attention: Library, Code IS-CAS-42B   1

National Aeronautics and Space Administration
Washington, D. C.   20546
Attention: Library, Code USS-10   1
                NASA Code RA   1

NASA Scientific and Technical Information Facility
P. O. Box 33   12
College Park, Maryland   20740   plus reproducible

Pennsylvania State University
233 Hammond Building
University Park, Pennsylvania   16802
Attention: Dr. Barnes McCormick   2

Massachusetts Institute of Technology
Aeroelastic and Structures Research Laboratory
Department of Aeronautics and Astronautics
Cambridge, Massachusetts   02139
Attention: Dr. Norman D. Ham   2

Sikorsky Aircraft
North Main Street
Stratford, Connecticut   06602
Attention: James Rorke   1

United Aircraft Research Laboratories
400 Main Street
East Hartford, Connecticut   06108
Attention: Jack Landgrebe   1

Rochester Applied Science Associates
100 Allens Creek Road
Rochester, New York   14618
Attention: Richard White   1

U. S. Army Aviation Materiel Laboratories
Aeromechanics Division
Fort Eustis, Virginia   23603
Attention: John Yeates   1

Army Aeronautical Research Laboratory
NASA Ames Research Center
Moffett Field, California   94035
Attention: Paul Yaggy, Technical Director   1

Bell Helicopter Company
P. O. Box 482
Fort Worth, Texas 76101
Attention: Watson Tanner   1

The Boeing Company
Vertol Division
P. O. Box 16858
Philadelphia, Pennsylvania 19142
Attention: Robert Spencer   1

U. S. Army Research Office
Engineering Sciences Division
Box CM, Duke Station
Durham, North Carolina 27706
Attention: Dr. Sudhir Kumar   1

Georgia Institute of Technology
School of Aerospace Engineering
Atlanta, Georgia 30332
Attention: E. R. Wood, Associate Professor of Aerospace
                 Engineering   1

Office of Naval Research
Department of the Navy
Air Programs (Code 461)
Washington, D. C. 20360
Attention: Thomas Wilson   1